



**A coupled surface-Cahn-Hilliard
bulk-diffusion system modeling lipid
raft formation in cell membranes**

Harald Garcke, Johannes Kampmann, Andreas Rätz
and Matthias Röger

Preprint Nr. 16/2015

A COUPLED SURFACE-CAHN–HILLIARD BULK-DIFFUSION SYSTEM MODELING LIPID RAFT FORMATION IN CELL MEMBRANES

HARALD GARCKE, JOHANNES KAMPMANN, ANDREAS RÄTZ, AND MATTHIAS RÖGER

ABSTRACT. We propose and investigate a model for lipid raft formation and dynamics in biological membranes. The model describes the lipid composition of the membrane and an interaction with cholesterol. To account for cholesterol exchange between cytosol and cell membrane we couple a bulk-diffusion to an evolution equation on the membrane. The latter describes a relaxation dynamics for an energy taking lipid-phase separation and lipid-cholesterol interaction energy into account. It takes the form of an (extended) Cahn–Hilliard equation. Different laws for the exchange term represent equilibrium and non-equilibrium models. We present a thermodynamic justification, analyze the respective qualitative behavior and derive asymptotic reductions of the model. In particular we present a formal asymptotic expansion near the sharp interface limit, where the membrane is separated into two pure phases of saturated and unsaturated lipids, respectively. Finally we perform numerical simulations and investigate the long-time behavior of the model and its parameter dependence. Both the mathematical analysis and the numerical simulations show the emergence of raft-like structures in the non-equilibrium case whereas in the equilibrium case only macrodomains survive in the long-time evolution.

1. INTRODUCTION

Phase separation processes that lead to microdomains of a well-defined length-scale below the system size arise in various physical and biological systems. A prominent example is the microphase separation in block-copolymers [7] or other soft materials, characterized by a fluid-like disorder on molecular scales and high degree of order at larger scales. Here micro-scale pattern arise by a competition between thermodynamic forces that drive (macro-)phase separation and entropic forces that limit phase separation. Different mathematical models for microphase separation in di-block copolymers have been developed, in particular built on self-consistent mean field theory (see for example [35] and the references therein) or density functional theory developed in [29, 39, 6] that leads to the so-called Ohta–Kawasaki free energy. Diblock-copolymer type models have also been studied on spheres and more general curved surfaces [32, 51, 10, 31] and show a variety of different stripe- or spot-like patterns. In contrast to materials science microphase separation on biological membranes is much less understood, in particular in living cells. In this contribution we present and analyze a model for so-called lipid rafts, that represent microdomains of specific lipid compositions.

The outer (plasma) membrane of a biological cell consists of a bilayer formed by several sorts of lipid molecules and contains various other molecules like proteins and cholesterol. Besides being the physical boundary of the cell the plasma membrane also plays an active part in the functioning of the cell. Many studies over the past decades have shown that the structure of the outer membrane is heterogeneous with several microdomains of different lipid and/or protein composition. Such domains have been clearly observed in artificial membranes such as giant unilamellar vesicles [48, 49]. Here a ‘less fluidic’ (liquid-ordered) phase of saturated lipids and cholesterol separates from a ‘more fluidic’ (liquid-disordered) phase of unsaturated lipids. The nucleation of dispersed microdomains is followed by a classical coarsening process that leads to

Date: September 1, 2015.

2010 Mathematics Subject Classification. 35K51, 35K71, 35Q92, 92C37, 35R37.

Key words and phrases. partial differential equations on surfaces, phase separation, Cahn–Hilliard equation, Ohta–Kawasaki energy, reaction-diffusion systems, singular limit.

coexisting domains with a length scale of the order of the system size. The situation is much more complex and much less understood for living cells. Their plasma membrane represents a heterogeneous structure with a complex and dynamic lipidic organization. The formation, maintenance and dynamics of intermediate-sized domains (10 - 200 nm on cells of μm size [30]) called ‘lipid rafts’ are of prime interest. These are characterized as liquid-ordered phases that consist of saturated lipids and are enriched of cholesterol and various proteins [44, 8]. These rafts contribute to various biological processes including signal transduction, membrane trafficking, and protein sorting [18]. It is therefore an interesting question to study the underlying process, by which these rafts are generated and maintained, and to understand the mechanism that allows for a dynamic distribution of intermediate-sized domains.

Several phenomenological mesoscale models have been proposed, see for example the review [18]. One class of models argues that raft formation is a result of a thermodynamic equilibrium process. Here one contribution is a phase separation energy that would induce a reduction of interfacial size between the raft and non-raft phases. The observation of nano-scale structures is then explained by including different additional energy contributions. One proposal is that thermal fluctuations near the critical temperature for the phase separation are responsible for the intermediate-sized structures. Other explanations consider interactions between lipids and membrane proteins that could act as a kind of surfactant or could ‘pin’ the interfaces due to their immobility [54, 46, 53]. Finally, raft formation could also be stabilized by induced changes of the membrane geometry and elasticity effects. However, as argued in [18], all such models are not able to reproduce key characteristics of raft dynamics; non-equilibrium effects essentially contribute to raft formation. Of particular importance are active transport processes of raft components that allow to maintain a non-equilibrium composition of the membrane. The competition between phase separation and recycling of raft components is argued to be of major importance for the dynamics and structure of lipid rafts.

Foret [20] proposed a simple mechanism of raft formation in a two-component fluid membrane. This model includes a constant exchange of lipids between the membrane and a lipid reservoir as well as a typical phase separation energy. While relaxation of the latter tends to create large domains, the constant insertion and extraction of lipids in the membrane ensures indeed the formation of rafts. The emerging microdomains are static (in contrast to the lipid rafts on actual cell membranes) and the size distribution of these rafts is rather uniform, whereas *in vivo* cell membranes show a dynamic distribution of rafts of different sizes (see the concluding remarks in [20] and the discussion of Forets model in [18]). Moreover, as already noticed in [18], whereas Forets model is motivated by including non-equilibrium effects his model can be equivalently characterized as relaxation dynamics for an effective energy given by the Ohta–Kawasaki energy of block-copolymers [39] that is well-known to generate phase-separation in intermediate-sized structures.

A similar model by Gómez, Sagués and Reigada [22] considers a ternary mixture of saturated and unsaturated lipids together with cholesterol and studies the interplay of lipid phase separation and a continuous recycling of cholesterol. An energy that is determined by the relative concentration ϕ of saturated lipids and the relative cholesterol concentration c is proposed that in particular includes a phase separation energy of Ginzburg–Landau type for the lipid phases and a preference for cholesterol–saturated lipid interactions over cholesterol–unsaturated lipid interactions. The dynamics include an exchange term for cholesterol that is given by an in-/out-flux proportional to the difference from a constant equilibrium concentration of cholesterol at the membrane.

Our aim here is to propose an extended model and to present both a mathematical analysis and numerical simulations. Similar as in [22] one ingredient of our model are energetic contributions from lipid phase separation and lipid-cholesterol interaction. In addition, we include the dynamics of cholesterol inside the cytosol (the liquid matter inside the cell) and prescribe a detailed coupling between the processes in the cell and on the cell membrane. In particular, the outflow

of cholesterol from the cytosol appears as a source-term in the membrane-cholesterol dynamic and will be characterized by a constitutive relation. We will investigate different choices of this relation and will illustrate the implications on the emergence of microdomains.

1.1. A lipid raft model including cholesterol exchange and cytosolic diffusion. To give a detailed description of our model let us fix an open bounded set $B \subset \mathbb{R}^3$ with smooth boundary $\Gamma = \partial B$ representing the cell volume and cell membrane, respectively. Let φ denote a rescaled relative concentration of saturated lipid molecules on the membrane, with $\varphi = 1$ and $\varphi = -1$ representing the pure saturated-lipid and pure unsaturated-lipid phases, respectively. Moreover let v denote the relative concentration of membrane-bound cholesterol, where $v = 1$ indicates maximal saturation, and let u denote the relative concentration of cytosolic cholesterol. We then prescribe a phase-separation and interaction energy of the form

$$(1.1) \quad \mathcal{F}(v, \varphi) = \int_{\Gamma} \left(\frac{\varepsilon}{2} |\nabla_{\Gamma} \varphi|^2 + \varepsilon^{-1} W(\varphi) + \frac{1}{2\delta} (2v - 1 - \varphi)^2 \right) d\mathcal{H}^2$$

with W a double-well potential that we choose as $W(\varphi) = \frac{1}{4}(1 - \varphi^2)^2$, constants $\varepsilon, \delta > 0$, and ∇_{Γ} denoting the surface gradient. The first two terms represent a classical Ginzburg-Landau phase separation energy, whereas the third term models a preferential binding of cholesterol to the lipid-saturated phase. We define the chemical potentials

$$(1.2) \quad \mu := \frac{\delta \mathcal{F}}{\delta \varphi} = -\varepsilon \Delta_{\Gamma} \varphi + \varepsilon^{-1} W'(\varphi) - \delta^{-1} (2v - 1 - \varphi),$$

$$(1.3) \quad \theta := \frac{\delta \mathcal{F}}{\delta v} = \frac{2}{\delta} (2v - 1 - \varphi),$$

where Δ_{Γ} denotes the Laplace–Beltrami operator on Γ , and prescribe for the dynamics of the concentrations over a time interval of observation $(0, T)$ the following system of equations

$$(1.4) \quad \partial_t u = D \Delta u \quad \text{in } B \times (0, T],$$

$$(1.5) \quad -D \nabla u \cdot \nu = q \quad \text{on } \Gamma \times (0, T],$$

$$(1.6) \quad \partial_t \varphi = \Delta_{\Gamma} \mu \quad \text{on } \Gamma \times (0, T],$$

$$(1.7) \quad \partial_t v = \Delta_{\Gamma} \theta + q = \frac{4}{\delta} \Delta_{\Gamma} v - \frac{2}{\delta} \Delta_{\Gamma} \varphi + q \quad \text{on } \Gamma \times (0, T],$$

where ν denotes the outer unit-normal field of B on Γ . The system is complemented with initial conditions u_0, φ_0, v_0 for u, φ and v , respectively. The first equation represents a simple diffusion equation for the cholesterol in the bulk, the second equation characterizes the outflow of cholesterol. The third equation is a Cahn–Hilliard dynamics for the lipid concentration on the membrane, whereas the equation for the cholesterol on the membrane combines a mass-preserving relaxation of the interaction energy and an exchange with the bulk reservoir of cholesterol given by the flux from the cytosol. This combination yields a diffusion equation with cross-diffusion contributions and a source term.

To close the system it remains to characterize the exchange term q . We follow here two possibilities: First we prescribe a constitutive relation by considering the membrane attachment as an elementary ‘reaction’ between free sites on the membrane and cholesterol, and the detachment as proportional to the membrane cholesterol concentration, expressed by the choice

$$(1.8) \quad q = c_1 u (1 - v) - c_2 v.$$

A similar coupling of bulk–surface equations has been investigated in a reaction-diffusion model for signaling networks [41, 42]. As a second possibility we consider choices of q that allow for a global free energy inequality for the coupled membrane/cytosol system. These two different cases could be considered as a distinction between open and closed systems and one important aspect of this work is to evaluate the consequences of these choices for the formation of complex phases.

We remark that the system conserves both the total cholesterol and the lipid concentrations since for arbitrary choices of q we obtain the relations

$$(1.9) \quad \frac{d}{dt} \left(\int_B u \, dx + \int_{\Gamma} v \, d\mathcal{H}^2 \right) = 0,$$

$$(1.10) \quad \frac{d}{dt} \int_{\Gamma} \varphi \, d\mathcal{H}^2 = 0.$$

Let us contrast the above model with the Ohta–Kawasaki model for phase separation in diblock copolymers mentioned above. Let $\Omega \subset \mathbb{R}^n$ denote a spatial domain, φ the relative concentration of one of the two polymers and let $m := \int \varphi$ be the prescribed average of φ over Ω . The mean field potential z is then given by

$$-\Delta z = \varphi - m \quad \text{in } \Omega, \quad \nabla z \cdot \nu_{\Omega} = 0 \quad \text{on } \partial\Omega, \quad \int_{\Omega} z = 0.$$

Then a free energy is prescribed of the form

$$(1.11) \quad \mathcal{F}_{OK}(\varphi) = \int_{\Omega} \left(\frac{\varepsilon}{2} |\nabla \varphi|^2 + \varepsilon^{-1} W(\varphi) \right) dx + \frac{\sigma}{2} \int_{\Omega} |\nabla z|^2 dx,$$

where $\sigma > 0$ is a fixed constant. Note that the last term can also be written as $\frac{\sigma}{2} \|\varphi - \int \varphi\|_{H^{-1}}^2$. A relaxation dynamics of Cahn–Hilliard type is then typically considered given as

$$(1.12) \quad \partial_t \varphi = \Delta \mu, \quad \mu = \frac{\delta \mathcal{F}_{OK}}{\delta \varphi} = -\varepsilon \Delta \varphi + \varepsilon^{-1} W'(\varphi) + \sigma z.$$

The energies \mathcal{F} and \mathcal{F}_{OK} both contain a Cahn–Hilliard type energy contribution that favors macro-phase separation but are different in the additional terms. However we will see below that stationary patterns for our lipid raft model with the choice (1.8) are for small $\delta > 0$ closely related to stationary points of \mathcal{F}_{OK} . If on the other hand one considers simple choices for q that lead to a global free energy inequality, we will observe a macro-scale separation of all saturated lipids in one connected domain. This indicates that in fact non-equilibrium processes are responsible for lipid raft formation.

Several asymptotic regimes are interesting in view of the different parameters included in our model. We will investigate the limit $\varepsilon \rightarrow 0$ that corresponds to a strong segregation limit and leads to a model where no mixing of the lipid phases is allowed and the domain splits into regions where $\varphi = 1$ and $\varphi = -1$ respectively. This limit corresponds to the sharp interface limit in phase-field models and connects to the analysis of the Ohta–Kawasaki model in [38]. Since the cytosolic diffusion in biological cells is known to be much faster than lateral diffusion on the cell membrane another natural reduction of the model appears in the limit $D \rightarrow \infty$ that leads to a non-local model defined solely on the cell membrane. Finally, assuming the effect of the lipid interaction with cholesterol to be large motivates to consider the asymptotic regime $\delta \downarrow 0$.

1.2. Outline of the paper and main results. In the next section we will derive the model (1.4)–(1.7) from thermodynamic considerations. In particular we will show that for arbitrary choices of the exchange term q the surface equations and the bulk (cytosolic) equations are thermodynamically consistent when viewed as separate systems. Depending on the specific choice of q we may or may not have a global (that is with respect to the full model) free energy inequality. We will present examples for both cases.

In Section 3 we will first derive a reduced raft model in the large cytosolic diffusion limit by formally taking $D \rightarrow \infty$. We then analyze the qualitative behavior of the (reduced) system in terms of a characterization of stationary points and an investigation of their relation to stationary points of the Ohta–Kawasaki model. A formal asymptotic expansion for the sharp interface reduction $\varepsilon \rightarrow 0$ of our raft model is presented in Section 4. Here we also briefly discuss the resulting limit problem that takes the form of a free boundary problem of Mullins–Sekerka type on the membrane with an additional coupling to a diffusion process in the bulk and including

an interaction with the cholesterol concentration. In Section 5 we present numerical simulations of the full and reduced raft model. In particular, we study spinodal decomposition, coarsening scenarios and the possible appearance of raft-like structures as (almost) stationary states for different choices of the exchange term q and for different parameter regimes. Some conclusions are stated in the final section.

2. THERMODYNAMIC JUSTIFICATION OF THE LIPID RAFT MODEL

In this section we will derive the governing equations for the lipid raft model from basic thermodynamical conservation laws using a free energy inequality. Our arguments are similar to an approach used by Gurtin [24, 25], who derived the Cahn-Hilliard equation in the context of non-equilibrium thermodynamics. We first of all consider the equations which have to hold on the surface, will then consider the equations in the bulk and subsequently we will couple both systems.

The basic quantities on the membrane surface are the rescaled relative concentration of the saturated lipid molecules φ , the concentration v of the membrane-bound cholesterol, the mass flux J_φ of the lipid molecules, the mass flux J_v of the cholesterol, the mass supply of cholesterol q , the surface free energy density f and the chemical potential μ related to the lipid molecules and the chemical potential θ related to the surface cholesterol. The underlying laws for any surface subdomain $\Sigma \subset \Gamma$ are the mass balance for the lipids

$$(2.1) \quad \frac{d}{dt} \int_{\Sigma} \varphi d\mathcal{H}^2 = - \int_{\partial\Sigma} J_\varphi \cdot n d\mathcal{H}^1,$$

the mass balance for the surface cholesterol

$$(2.2) \quad \frac{d}{dt} \int_{\Sigma} v d\mathcal{H}^2 = - \int_{\partial\Sigma} J_v \cdot n d\mathcal{H}^1 + \int_{\Sigma} q d\mathcal{H}^2$$

and the second law of thermodynamics, which in the isothermal situation has the form

$$(2.3) \quad \frac{d}{dt} \int_{\Sigma} f d\mathcal{H}^2 \leq - \int_{\partial\Sigma} (\mu J_\varphi \cdot n - (\partial_t \varphi f_{,\nabla_\Gamma \varphi} \cdot n) + \theta J_v \cdot n) d\mathcal{H}^1 + \int_{\Sigma} \theta q d\mathcal{H}^2$$

where f denotes the surface free energy density and where n is the outer unit conormal to $\partial\Sigma$ in the tangent space of Γ . In addition, we denote by $d\mathcal{H}^d$ the integration with respect to the d -dimensional surface measure and $f_{,\nabla_\Gamma \varphi}$ denotes the partial derivatives of f with respect to the variables related to $\nabla_\Gamma \varphi$ in a constitutive relation $f = f(\dots, \nabla_\Gamma \varphi, \dots)$. Similarly we will denote with a subscript comma partial derivatives with respect to other variables. For a discussion of these laws in cases in which source terms are present and at the same time f does not depend on $\nabla_\Gamma \varphi$ we refer to [24], [26, Chapter 62], and [40]. Thermodynamical models of phase transitions with an order parameter typically involve a free energy density f which does depend on $\nabla_\Gamma \varphi$. In this case the free energy flux does not only involve the classical terms μJ_φ and θJ_v but also a term $\partial_t \varphi f_{,\nabla_\Gamma \varphi}$. This is discussed in [25, 5, 2]. Gurtin [25] introduces a microforce balance involving a microstress ξ in order to derive the Cahn-Hilliard equation. Here, we do not discuss the microforce balance and instead already use the form $\xi = f_{,\nabla_\Gamma \varphi}$ which could be derived in our context in the same way as in [25]. However, in order to shorten the presentation we do not state the details. We hence obtain (2.3) as the relevant free energy inequality in cases where no external microforces are present.

Since the above (in-)equalities (2.1)–(2.3) hold for all Σ , we obtain with the help of the Gauß theorem on surfaces the local forms, compare [25],

$$(2.4) \quad \partial_t \varphi + \operatorname{div}_\Gamma J_\varphi = 0 \quad \text{in } \Gamma \times (0, T],$$

$$(2.5) \quad \partial_t v + \operatorname{div}_\Gamma J_v = q \quad \text{in } \Gamma \times (0, T],$$

$$(2.6) \quad \partial_t f + \operatorname{div}_\Gamma (\mu J_\varphi - \partial_t \varphi f_{,\nabla_\Gamma \varphi} + \theta J_v) \leq \theta q \quad \text{in } \Gamma \times (0, T].$$

With the constitutive relation $f = f(v, \varphi, \nabla_\Gamma \varphi)$ we obtain from the local form of the free energy inequality

$$f_{,\varphi} \partial_t \varphi + f_{,v} \partial_t v + \nabla_\Gamma \mu \cdot J_\varphi + \nabla_\Gamma \theta \cdot J_v + (\operatorname{div}_\Gamma J_\varphi) \mu + (\operatorname{div}_\Gamma J_v) \theta - \partial_t \varphi \operatorname{div}_\Gamma f_{,\nabla_\Gamma \varphi} \leq \theta q.$$

Using the conservation laws (2.4) and (2.5) we obtain

$$(f_{,\varphi} - \operatorname{div}_\Gamma(f_{,\nabla_\Gamma \varphi}) - \mu) \partial_t \varphi + (f_{,v} - \theta) \partial_t v + \nabla_\Gamma \mu \cdot J_\varphi + \nabla_\Gamma \theta \cdot J_v \leq 0.$$

The fact that solutions of the conservation laws with arbitrary values for $\partial_t \varphi$ and $\partial_t v$ can appear is used in the theory of rational thermodynamics to show that the factors multiplying $\partial_t \varphi$ and $\partial_t v$ have to disappear as they do not depend on $\partial_t \varphi$ and $\partial_t v$. We refer to Liu's method of Lagrange multipliers [34] and to [26, 5] for a more precise discussion on how the free energy inequality can be used to restrict possible constitutive relations. We now choose the following constitutive relations which guarantee that the free energy inequality is fulfilled for arbitrary solutions of (2.4), (2.5). In fact, choosing

$$(2.7) \quad \mu = f_{,\varphi} - \operatorname{div}_\Gamma(f_{,\nabla_\Gamma \varphi}),$$

$$(2.8) \quad \theta = f_{,v},$$

$$(2.9) \quad J_\varphi = -D_\varphi \nabla_\Gamma \mu,$$

$$(2.10) \quad J_v = -D_v \nabla_\Gamma \theta$$

with $D_\varphi, D_v \geq 0$ ensures that the free energy inequality is fulfilled for all solutions of the conservation laws. More general models, e.g. taking cross diffusion into account, are possible and we refer to [5] for an approach which can be used to obtain more general models.

We now consider the governing physical laws in the bulk. As variables we choose u which is the relative concentration of the cytosolic cholesterol, the bulk chemical potential μ_u , the bulk free energy density $f_b(u)$, the bulk flux J_u and the surface mass source term q_u . We need to fulfill the following mass balance equation in integral form which has to hold for all open $U \subset B$:

$$(2.11) \quad \frac{d}{dt} \int_U u \, dx = - \int_{(\partial U) \setminus \Gamma} J_u \cdot \nu \, d\mathcal{H}^2 + \int_{(\partial U) \cap \Gamma} q_u \, d\mathcal{H}^2$$

and the free energy inequality

$$(2.12) \quad \frac{d}{dt} \int_U f_b(u) \, dx \leq - \int_{(\partial U) \setminus \Gamma} \mu_u J_u \cdot \nu \, d\mathcal{H}^2 + \int_{(\partial U) \cap \Gamma} \mu_u q_u \, d\mathcal{H}^2$$

which also has to hold for all open $U \subset B$. Here we allowed for a source term q_u on Γ and in accordance to our discussion above we introduced the free energy source $\mu_u q_u$ in (2.12). As on the interface the free energy source term is given classically as a product of the mass source term and the chemical potential. If we use the fact that we can choose an arbitrary open set U which is compactly supported in B (which then implies $(\partial U) \cap \Gamma = \emptyset$) we obtain with the help of the Gauß theorem

$$(2.13) \quad \partial_t u + \operatorname{div} J_u = 0 \quad \text{in } B \times (0, T],$$

$$(2.14) \quad \partial_t f_b(u) + \operatorname{div}(\mu_u J_u) \leq 0 \quad \text{in } B \times (0, T].$$

Choosing

$$(2.15) \quad \mu_u = f'_b(u),$$

$$(2.16) \quad J_u = -M(u) \nabla(f'_b(u))$$

makes sure that (2.14) is true for all solutions of (2.13). In the following we will often choose $M(u) = \frac{D_u}{f''_b(u)}$ and this will lead to the linear diffusion equation (1.4)

$$\partial_t u - D_u \Delta u = 0 \quad \text{in } B \times (0, T].$$

Choosing U such that $\partial U \cap \Gamma \neq \emptyset$ we obtain from (2.11)

$$0 = \int_U (\partial_t u + \operatorname{div} J_u) dx = \int_{\partial U \cap \Gamma} (q_u + J_u \cdot \nu) d\mathcal{H}^2$$

which gives, since U is arbitrary,

$$q_u = -J_u \cdot \nu (= D_u \nabla u \cdot \nu) \quad \text{in } \Gamma \times (0, T],$$

and which yields (1.5) for $q = -q_u$. We will now state global balance laws in the case where the mass supply for the interface stems from the bulk and vice versa.

Lemma 2.1. *We assume that the above stated mass balance equations hold for the bulk and the surface and assume in addition that $q_u = -q$. Then it holds*

$$\frac{d}{dt} \left(\int_B u dx + \int_\Gamma v d\mathcal{H}^2 \right) = 0 \quad \frac{d}{dt} \int_\Gamma \varphi d\mathcal{H}^2 = 0.$$

If in addition, the free energy inequalities in the bulk and on the surface are true it also holds

$$\frac{d}{dt} \left(\int_\Gamma f(v, \varphi, \nabla_\Gamma \varphi) d\mathcal{H}^2 + \int_B f_b(u) dx \right) \leq \int_\Gamma q(\theta - \mu_u) d\mathcal{H}^2.$$

Proof. The first two equations follow from (2.1), (2.2) with $\Sigma = \Gamma$ and (2.11) with $U = B$ since $\partial U = \Gamma$ and since $\partial \Gamma = \emptyset$. The total free energy inequality follows similarly from (2.3) and (2.12). \square

Remark 2.2. (i) In the above lemma we chose $q_u = -q$, that is the mass lost on the surface generates a source of mass for the bulk.

(ii) Several constitutive laws for q make sense. It is possible to consider

$$(2.17) \quad q = -c(\theta - \mu_u), \quad c \geq 0$$

which leads to model for which the total free energy decreases. In this case we obtain

$$\frac{d}{dt} \left(\int_\Gamma f(v, \varphi, \nabla_\Gamma \varphi) d\mathcal{H}^2 + \int_B f_b(u) dx \right) \leq - \int_\Gamma c(\theta - \mu_u)^2 d\mathcal{H}^2 \leq 0.$$

(iii) We also consider the reaction type source term, compare (1.8),

$$q = c_1 u(1 - v) + c_2 v.$$

Also in this case we obtain a consistent model which fulfills the bulk and surface free energy inequalities with source terms as stated above. However, in this case the total free energy as the sum of the bulk and the surface free energy might increase which can be due to the fact that we neglect energy contributions generated by the detachment and attachment process.

(iv) One possible choice for the surface free energy density is, compare (1.1),

$$f(v, \varphi, \nabla_\Gamma \varphi) = \frac{\gamma \varepsilon}{2} |\nabla_\Gamma \varphi|^2 + \frac{\gamma}{\varepsilon} W(\varphi) + \frac{1}{2\delta} (2v - 1 - \varphi)^2, \quad \varepsilon, \delta, \gamma > 0.$$

For $f_b(u) = \frac{1}{2}u^2$, $q_u = -q$ and $D_u = D$, $\gamma = D_\varphi = D_v = 1$ we obtain the system (1.2)–(1.7).

With the above quadratic choice for f_b and arguing as in the derivation of the energy inequality one can prove the identity

$$(2.18) \quad \begin{aligned} \frac{d}{dt} \left(\int_\Gamma \frac{\varepsilon}{2} |\nabla_\Gamma \varphi|^2 + \frac{1}{\varepsilon} W(\varphi) + \frac{1}{2\delta} (2v - 1 - \varphi)^2 d\mathcal{H}^2 + \int_B \frac{1}{2} u^2 dx \right) \\ + \int_\Gamma (|\nabla_\Gamma \mu|^2 + |\nabla_\Gamma \theta|^2) d\mathcal{H}^2 + \int_B D |\nabla u|^2 = \int_\Gamma q(\theta - u) \end{aligned}$$

where the last term is non-positive for the choice (2.17). Any other evolution that is based on a choice of q such that the right-hand side of (2.18) is always non-positive decreases the

total free energy. This is in particular the case for choices of q such that (1.2)-(1.7) can be characterized as a gradient flow.

In the following we are mainly interested in the dependence on the parameters ε, δ, D_u and therefore as in (iv) above we always set $D_u = D, \gamma = D_\varphi = D_v = 1$, in which case the above choices of free energy densities and mass fluxes yield the system (1.2)-(1.7).

3. QUALITATIVE BEHAVIOR

In this section we will investigate qualitative properties of the model (1.2)-(1.7) and of the asymptotic reduction in the large cytosolic diffusion limit that we derive below. One key question here is whether or not our lipid raft model supports the formation of mesoscale patterns. We will distinguish different choices for the exchange term q and compare evolutions that reduce the total free energy with the evolution for the choice q given by the reaction-type law (1.8), which we consider as a prototype of a non-equilibrium model. We remark that most of the arguments in this section are purely formal; a rigorous justification is out of the scope of the present paper. In particular, we assume the existence of smooth solutions, their convergence to stationary states as times tends to infinity, and that the long-time behavior of the full system asymptotically agrees with that of the reduced system developed below.

We first observe that under an additional growth assumption on the exchange term q we obtain energy bounds, even in the case that the system does not satisfy a global energy inequality.

Proposition 3.1. *Assume that q has at most linear growth, that is there exists $\Lambda > 0$ such that*

$$(3.1) \quad |q(\varphi, u, v)| \leq \Lambda(1 + |\varphi| + |u| + |v|) \quad \text{for all } \varphi, u, v \in \mathbb{R}.$$

Then for all $0 < t < T$ and all $D \geq D_0 > 0, 0 < \varepsilon \leq \varepsilon_0$ any solution of (1.2)-(1.7) with initial data φ_0, u_0, v_0 satisfies

$$(3.2) \quad \mathcal{F}(v(\cdot, t), \varphi(\cdot, t)) + \frac{1}{2} \int_B u(\cdot, t)^2 + \int_0^t \int_B \frac{D}{2} |\nabla u|^2 \leq C(\delta, \Lambda, T, D_0, \varepsilon_0, v_0, \varphi_0, u_0).$$

Proof. From (2.18) we deduce that

$$(3.3) \quad \begin{aligned} & \frac{d}{dt} \left(\mathcal{F}(v(\cdot, t), \varphi(\cdot, t)) + \frac{1}{2} \int_B u(\cdot, t)^2 \right) \\ &= - \int_B D |\nabla u|^2(\cdot, t) - \int_\Gamma [|\nabla_\Gamma \mu|^2(\cdot, t) + |\nabla_\Gamma \theta|^2(\cdot, t) - (\theta - u)(\cdot, t) q(\varphi(\cdot, t), u(\cdot, t), v(\cdot, t))]. \end{aligned}$$

For the last term we use the estimate

$$(3.4) \quad \begin{aligned} \left| \int_\Gamma (\theta - u) q(\varphi, u, v) \right| &\leq \int_\Gamma \left(\theta^2 + u^2 + C_\Lambda (1 + \varphi^2 + u^2 + v^2) \right) \\ &= \int_\Gamma \theta^2 + C_\Lambda \int_\Gamma (1 + \varphi^2) + (C_\Lambda + 1) \int_\Gamma u^2 + C_\Lambda \int_\Gamma v^2. \end{aligned}$$

For the second term on the right-hand side we obtain

$$(3.5) \quad \int_\Gamma (1 + \varphi^2) \leq C(1 + \int_\Gamma W(\varphi)) \leq C(\varepsilon_0)(1 + \mathcal{F}(v(\cdot, t), \varphi(\cdot, t))).$$

Using [28, Chapter 2, (2.25)] the third term on the right-hand side of (3.4) can be estimated by bulk quantities,

$$\int_\Gamma u^2 \leq \frac{D}{2} \int_B |\nabla u|^2 + C(D) \int_B u^2$$

for a suitable constant $C(D)$, which in particular yields for all $D \geq D_0$

$$(3.6) \quad \int_\Gamma u^2 \leq \frac{D}{2} \int_B |\nabla u|^2 + C(D_0) \int_B u^2.$$

To estimate the last integral on the right-hand side of (3.4) we first use Young's inequality and (1.3) to obtain

$$\frac{16}{\delta^2}v^2 = \theta^2 + \frac{4}{\delta}\theta(1 + \varphi) + \frac{4}{\delta^2}(1 + \varphi)^2 \leq 2\theta^2 + \frac{8}{\delta^2}(1 + \varphi)^2,$$

and further deduce that

$$(3.7) \quad v^2 \leq \frac{\delta^2}{8}\theta^2 + C(1 + W(\varphi)),$$

$$\int_{\Gamma} v^2(\cdot, t) \leq C(\delta, \varepsilon_0) \left(1 + \mathcal{F}(v(\cdot, t), \varphi(\cdot, t))\right).$$

We therefore obtain from (3.3)-(3.7) that

$$\begin{aligned} & \frac{d}{dt} \left(\mathcal{F}(v(\cdot, t), \varphi(\cdot, t)) + \frac{1}{2} \int_B u(\cdot, t)^2 \right) + \frac{D}{2} \int_B |\nabla u|^2(\cdot, t) + \int_{\Gamma} \left(|\nabla_{\Gamma} \mu|^2(\cdot, t) + |\nabla_{\Gamma} \theta|^2(\cdot, t) \right) \\ & \leq C(\delta, \Lambda, D_0, \varepsilon_0) \left(\mathcal{F}(v(\cdot, t), \varphi(\cdot, t)) + \frac{1}{2} \int_B u(\cdot, t)^2 \right) + C(\delta, \Lambda). \end{aligned}$$

By the Gronwall inequality we deduce the claim. \square

Note that for the choice (1.8) of q assumption (3.1) is not satisfied. However, for any modification that coincides with that choice on a bounded domain in the u, v plane and that has at most linear growth outside the conclusion of Proposition 3.1 holds. For (2.17) or any other choice of q that implies a total free energy inequality we obtain an even better estimate, since now the right-hand side in (2.18) is non-positive.

3.1. A reduced model in the limit of large cytosolic diffusion. Since in the application to cell biology the bulk (cytosolic) diffusion is much higher than the lateral membrane diffusion a reasonable reduction of the model can be expected in the limit $D \rightarrow \infty$. In the case that the exchange term q satisfies assumption (3.1) we deduce by Proposition 3.1 that $\int_0^T \int_B D |\nabla u|^2$ is bounded uniformly in D . The same conclusion holds in the case of any free-energy decreasing evolution by (2.18). Therefore in the formal limit $D \rightarrow \infty$ we conclude that u is spatially constant and obtain the (non-local) system of surface PDEs

$$(3.8) \quad \partial_t \varphi = \Delta_{\Gamma} \mu \quad \text{on } \Gamma \times (0, T],$$

$$(3.9) \quad \mu = -\varepsilon \Delta_{\Gamma} \varphi + \varepsilon^{-1} W'(\varphi) - \delta^{-1} (2v - 1 - \varphi) \quad \text{on } \Gamma \times (0, T],$$

$$(3.10) \quad \partial_t v = \Delta_{\Gamma} \theta + q = \frac{4}{\delta} \Delta_{\Gamma} v - \frac{2}{\delta} \Delta_{\Gamma} \varphi + q(\varphi, u, v) \quad \text{on } \Gamma \times (0, T].$$

This system is complemented by initial conditions for φ and v . The cholesterol concentration $u = u(t)$ is determined by a mass conservation condition

$$(3.11) \quad \int_B u(t) + \int_{\Gamma} v(\cdot, t) = M,$$

where $M > 0$ is the total mass of cholesterol in the system.

Note that the transformation of the coupled bulk-surface system into a system only defined in the surface has the price of introducing a non-local term by the characterization of u through the mass constraint. The reduction (3.8)-(3.11) is similar to the reduction to a shadow system for 2×2 reaction-diffusion systems introduced by Keener [27], see also the discussion in [37].

In the qualitative analysis below and the numerical simulations we will often restrict ourselves to the special choice q of the exchange function given in (1.8). For the reduced model it is then possible to compute the evolution of the total mass of u and v , which are related by (3.11). We

deduce, cf. (2.11),

$$\begin{aligned}
(3.12) \quad \frac{d}{dt} \int_B u(t) dx &= - \int_{\Gamma} q(\varphi(\cdot, t), u(t), v(\cdot, t)) d\mathcal{H}^2 = \int_{\Gamma} -c_1 u(t)(1-v)(\cdot, t) + c_2 v(\cdot, t) d\mathcal{H}^2 \\
&= \int_{\Gamma} (c_1 u(t) + c_2) v(\cdot, t) d\mathcal{H}^2 - c_1 \frac{|\Gamma|}{|B|} \int_B u(t) dx \\
&= (c_1 u(t) + c_2) \left(M - \int_B u(t) dx \right) - c_1 \frac{|\Gamma|}{|B|} \int_B u(t) dx \\
&= -\frac{c_1}{|B|} \left(\int_B u(t) dx \right)^2 + \left(c_1 \frac{M - |\Gamma|}{|B|} - c_2 \right) \int_B u(t) dx + c_2 M
\end{aligned}$$

and therefore we see that $u(t)$ remains nonnegative if it was initially nonnegative (which is the relevant case) and converges for $t \rightarrow \infty$ to u_{∞} , which is the positive zero of

$$p(z) = -c_1 z^2 + \left(c_1 \frac{M - |\Gamma|}{|B|} - c_2 \right) z + \frac{c_2 M}{|B|},$$

thus

$$(3.13) \quad u_{\infty} = \frac{1}{2} \left(\frac{M - |\Gamma|}{|B|} - \frac{c_2}{c_1} \right) + \sqrt{\frac{1}{4} \left(\frac{M - |\Gamma|}{|B|} - \frac{c_2}{c_1} \right)^2 + \frac{c_2 M}{c_1 |B|}}.$$

Since $p(0) > 0$ and $p(\frac{M}{|B|}) < 0$ we also obtain that $\int_{\Gamma} v(t)$ remains in $[0, M]$ for all times.

We remark that if q is given as in (1.8), then assumption (3.1) does not hold. Nevertheless we can obtain the reduced model for this particular choice of q if we start with a modified version: Replace first q by

$$\tilde{q}(u, v) = c_1 u - c_1 \eta(u) v - c_2 v,$$

where $\eta : \mathbb{R} \rightarrow \mathbb{R}$ is any smooth, monotone increasing and uniformly bounded function with $\eta(r) = r$ for $|r| \leq M|B|^{-1}$. Now the above arguments apply and we obtain the non-local model with exchange term \tilde{q} . By analogous computations as above we then deduce

$$\frac{d}{dt} \int_B u(t) dx = -\frac{c_1 |\Gamma|}{|B|} \int_B u(t) dx + \left(c_1 \eta \left(\frac{1}{|B|} \int_B u(t) dx \right) + c_2 \right) \left(M - \int_B u(t) dx \right),$$

which yields $0 \leq \int_B u(t) dx \leq M$ for all $t \geq 0$ if this property holds for the initial data. But this implies $\tilde{q}(u(t), v(\cdot, t)) = q(u(t), v(\cdot, t))$ for all $t \geq 0$. This justifies to consider in the following analysis and in the numerical simulations in Section 5 the exchange term q from (1.8) also for the non-local reduction.

3.2. Stationary points. We are in particular interested in the long-time behavior of solutions and will therefore next investigate stationary points of our lipid raft system. For the full system (1.2)-(1.7) stationary points $(\varphi_{\infty}, u_{\infty}, v_{\infty})$ are characterized by the equations

$$\begin{aligned}
(3.14) \quad 0 &= \Delta_{\Gamma} \mu_{\infty} \quad \text{on } \Gamma, \\
0 &= \Delta_{\Gamma} \theta_{\infty} + q(\varphi_{\infty}, u_{\infty}, v_{\infty}) \quad \text{on } \Gamma, \\
\Delta u_{\infty} &= 0 \quad \text{in } B, \quad -D\nabla u_{\infty} \cdot \nu = q(\varphi_{\infty}, u_{\infty}, v_{\infty}) \quad \text{on } \Gamma.
\end{aligned}$$

This implies that μ_{∞} is constant and

$$(3.15) \quad -\varepsilon \Delta_{\Gamma} \varphi_{\infty} + \frac{1}{\varepsilon} W'(\varphi_{\infty}) = \frac{1}{\delta} (2v_{\infty} - 1 - \varphi_{\infty}) + \mu_{\infty} = \frac{\theta_{\infty}}{2} + \mu_{\infty},$$

$$(3.16) \quad q(\varphi_{\infty}, u_{\infty}, v_{\infty}) = -\frac{2}{\delta} \Delta (2v_{\infty} - 1 - \varphi_{\infty}),$$

$$(3.17) \quad \Delta u_{\infty} = 0 \quad \text{in } B, \quad -D\nabla u_{\infty} \cdot \nu = q(\varphi_{\infty}, u_{\infty}, v_{\infty}) \quad \text{on } \Gamma.$$

Alternatively, this system can be characterized by

$$(3.18) \quad -\varepsilon \Delta_{\Gamma} \varphi_{\infty} + \frac{1}{\varepsilon} W'(\varphi_{\infty}) = \mathcal{Q}(\varphi_{\infty}) + \mu_{\infty},$$

where $\mathcal{Q}(\varphi_{\infty}) = \frac{1}{2} \theta_{\infty}$ is a nonlocal function of φ_{∞} as u_{∞}, v_{∞} and hence θ_{∞} are determined by φ_{∞} through (3.16), (3.17).

3.3. The case of an energy-decreasing evolution. Let us in the following first consider the case that q is chosen such that the right-hand side in (2.18) is nonpositive, hence the total free energy is decreasing. For any stationary point $u_{\infty}, v_{\infty}, \varphi_{\infty}$ the energy inequality (2.18) yields that $\mu_{\infty}, \theta_{\infty}$ and u_{∞} are constant, in particular by (3.15)

$$\begin{aligned} -\varepsilon \Delta_{\Gamma} \varphi_{\infty} + \frac{1}{\varepsilon} W'(\varphi_{\infty}) &= \frac{\theta_{\infty}}{2} + \mu_{\infty} \in \mathbb{R}, \\ q(\varphi_{\infty}, u_{\infty}, v_{\infty}) &= 0. \end{aligned}$$

In addition, we fix the total lipid and cholesterol masses as they are for any evolution determined by the initial conditions. We therefore prescribe, for M, M_1 given,

$$\begin{aligned} M &= \int_B u_{\infty} + \int_{\Gamma} v_{\infty} = |B|u_{\infty} + \int_{\Gamma} v_{\infty}, \\ M_1 &= \int_{\Gamma} \varphi_{\infty}. \end{aligned}$$

In particular, the stationary state φ_{∞} coincides with a critical point of the Cahn–Hilliard energy subject to a volume constraint. The condition $q = 0$ provides an additional relation between $\varphi_{\infty}, u_{\infty}$ and v_{∞} . In the case of the exchange law (2.17) this determines $\int_{\Gamma} v_{\infty}$ and θ_{∞} .

We can elaborate the connection with stationary points of the Cahn–Hilliard equation a bit more if we in addition assume that $(u_{\infty}, v_{\infty}, \varphi_{\infty})$ is a local minimizer of the energy (1.1). We represent the latter as

$$(3.19) \quad \mathcal{F}(v, \varphi) = \mathcal{F}_1(\varphi) + \mathcal{F}_2(v, \varphi),$$

where

$$\mathcal{F}_1(\varphi) := \int_{\Gamma} \frac{\varepsilon}{2} |\nabla \varphi|^2 + \varepsilon^{-1} W(\varphi), \quad \mathcal{F}_2(v, \varphi) := \int_{\Gamma} \frac{1}{2\delta} (2v - 1 - \varphi)^2.$$

We also assume that both $\int_{\Gamma} \varphi_{\infty}$ and $\int_{\Gamma} v_{\infty}$ are fixed by the initial data and the condition $q = 0$, which holds in particular in case of the exchange law (2.17).

For any v, φ with $\int_{\Gamma} v = \int_{\Gamma} v_{\infty}$ and $\int_{\Gamma} \varphi = \int_{\Gamma} \varphi_{\infty}$ we then have

$$\begin{aligned} \int_{\Gamma} (2v - 1 - \varphi)^2 &= \int_{\Gamma} \left(2v - 1 - \varphi - \int_{\Gamma} (2v - 1 - \varphi) \right)^2 + \int_{\Gamma} \left(\int_{\Gamma} (2v - 1 - \varphi) \right)^2 \\ &\geq \int_{\Gamma} \left(\int_{\Gamma} (2v_{\infty} - 1 - \varphi_{\infty}) \right)^2 \end{aligned}$$

and deduce that under the respective mass constraints the minimizer of $\mathcal{F}_2(v, \varphi)$ are given by those (v, φ) for which $2v - 1 - \varphi$ is constant, and that the minimum only depends on $\int_{\Gamma} v$ and $\int_{\Gamma} \varphi$. Since θ_{∞} and thus $2v_{\infty} - 1 - \varphi_{\infty}$ are constant, we see that $u_{\infty}, v_{\infty}, \varphi_{\infty}$ minimizes \mathcal{F}_2 .

Moreover, for any φ satisfying the mass constraint the minimum of \mathcal{F}_2 is attained by $v = \frac{1}{2}(1 + \varphi + \int_{\Gamma} (2v - 1 - \varphi))$ and is independent of φ . Therefore φ_{∞} as above needs to be a local minimizer of the Cahn–Hilliard energy \mathcal{F}_1 subject to a given mass constraint. In the case of the Cahn–Hilliard dynamics in an open convex set in \mathbb{R}^n , it is known [45] that stable stationary points converge in the sharp interface limit $\varepsilon \rightarrow 0$ to configurations with one connected phase boundary of constant curvature. In analogy, one therefore might expect that for $\varepsilon > 0$ sufficiently small the only local minimizer in our lipid raft model for choices q that lead to an energy-decreasing evolution are given by configurations with one lipid phase concentrated in a single geodesic ball

on Γ . In particular, such local minimizer do not represent mesoscale pattern like lipid rafts. In Section 5.3.4 we present a numerical simulation for energy decreasing dynamics that confirms the expected behavior.

3.4. The case of the exchange term (1.8). Let us next discuss the choice of q as given in (1.8). The representation (3.18) shows some similarity to the equation for stationary points of the Ohta–Kawasaki model described above. We can make this more transparent in the case of the reduced system (3.8)–(3.11), at least if we presume that the long term behavior of the reduced systems captures the respective behavior of the full system (which means that the order of limits $D \rightarrow \infty$ and $t \rightarrow \infty$ can be interchanged). Since u_∞ is constant we obtain, writing $\tilde{c}_1 = c_1 u_\infty$ for convenience, that

$$(3.20) \quad 0 = \int_{\Gamma} q(u_\infty, v_\infty) = |\Gamma| \tilde{c}_1 - (\tilde{c}_1 + c_2) \int_{\Gamma} v_\infty$$

and further

$$\begin{aligned} q(u_\infty, v_\infty) &= -\frac{\tilde{c}_1 + c_2}{2}(v_\infty - 1 - \varphi_\infty) - \frac{\tilde{c}_1 + c_2}{2}(1 + \varphi_\infty) + \tilde{c}_1 \\ &= -\frac{\delta(\tilde{c}_1 + c_2)}{4}\theta_\infty - \frac{\tilde{c}_1 + c_2}{2}(1 + \varphi_\infty) + \tilde{c}_1 \\ &= -\frac{\delta(\tilde{c}_1 + c_2)}{4}\left(\theta_\infty - \int \theta_\infty\right) - \frac{\delta(\tilde{c}_1 + c_2)}{4} \frac{2}{\delta} \int (v_\infty - 1 - \varphi_\infty) - \frac{\tilde{c}_1 + c_2}{2}(1 + \varphi_\infty) + \tilde{c}_1 \\ &= -\frac{\delta(\tilde{c}_1 + c_2)}{4}\left(\theta_\infty - \int \theta_\infty\right) - \frac{\tilde{c}_1 + c_2}{2}\left(\varphi_\infty - \int \varphi_\infty\right), \end{aligned}$$

where we have used (3.20) in the third line. This implies by (3.14)

$$\left(-\Delta_\Gamma + \frac{\delta(\tilde{c}_1 + c_2)}{4}\right)\left(\theta_\infty - \int \theta_\infty\right) = -\frac{\tilde{c}_1 + c_2}{2}\left(\varphi_\infty - \int \varphi_\infty\right).$$

Since μ_∞ is constant we deduce from equation (3.18)

$$\begin{aligned} -\varepsilon \Delta_\Gamma \varphi_\infty + \varepsilon^{-1} W'(\varphi_\infty) &= \mu_\infty + \frac{1}{2} \int \theta_\infty + \frac{1}{2} \left(\theta_\infty - \int \theta_\infty\right) \\ &= \mu_\infty + \frac{1}{2} \int \theta_\infty - \frac{\tilde{c}_1 + c_2}{4} \left(-\Delta_\Gamma + \frac{\delta(\tilde{c}_1 + c_2)}{4}\right)^{-1} \left(\varphi_\infty - \int \varphi_\infty\right). \end{aligned}$$

For $\delta \ll 1$ this can be approximated by

$$(3.21) \quad -\varepsilon \Delta_\Gamma \varphi_\infty + \varepsilon^{-1} W'(\varphi_\infty) + \frac{\tilde{c}_1 + c_2}{4} (-\Delta_\Gamma)^{-1} \left(\varphi_\infty - \int \varphi_\infty\right) = \mu_\infty + \frac{1}{2} \int \theta_\infty.$$

The latter equation corresponds to stationary points of the Ohta–Kawasaki functional

$$(3.22) \quad \mathcal{F}_{OK}(\varphi) = \int_{\Gamma} \left(\frac{\varepsilon}{2} |\nabla \varphi|^2 + \varepsilon^{-1} W(\varphi)\right) + \frac{\sigma}{2} \|\varphi - \int \varphi\|_{H^{-1}}^2$$

with

$$(3.23) \quad \sigma = \frac{\tilde{c}_1 + c_2}{4},$$

where the constant on the right-hand side of (3.21) should be interpreted as a Lagrange multiplier associated to a mass constraint for φ .

The total lipid mass $\int \varphi$ is given by the initial data. We can also identify $\tilde{c}_1 + c_2$ as a function of the data. First its value is characterized by u_∞ and using (3.13) we deduce

$$(3.24) \quad \tilde{c}_1 + c_2 = \frac{1}{2} \left(c_2 + \frac{M}{|B|} c_1 - \frac{|\Gamma|}{|B|} c_1\right) + \sqrt{\frac{1}{4} \left(c_2 + \frac{M}{|B|} c_1 - \frac{|\Gamma|}{|B|} c_1\right)^2 + c_1 c_2 \frac{|\Gamma|}{|B|}}.$$

In Section 5.3.2 we will present simulations that confirm that the long-time behavior of the reduced system is for $\delta \ll 1$ in fact very close to that of the Ohta–Kawasaki dynamics. In particular, in contrast to any choice of q that induces an energy-decreasing evolution, in the case of the exchange term (1.8) we in fact see the occurrence of mesoscale patterns.

Remark 3.2. Let us highlight one key difference in the long-time behavior of our model in the different cases considered above. For a free-energy decreasing evolution stationary states are characterized by the properties that θ_∞ is constant and $q_\infty = q(\varphi_\infty, u_\infty, v_\infty)$ zero. For the choice (1.8) of the exchange term on the other hand and the reduced system we have stationary states with non-vanishing q_∞ , which correspond to an persisting exchange of cholesterol between bulk and cell membrane. This process eventually allows for the formation of complex pattern on a mesoscopic scale.

4. SHARP INTERFACE LIMIT $\varepsilon \rightarrow 0$ BY FORMALLY MATCHED ASYMPTOTIC EXPANSIONS

In this section we formally derive the sharp interface limit of the diffuse interface model (1.2)–(1.7) as $\varepsilon \rightarrow 0$. We assume throughout this section that the tuple $(u_\varepsilon, \varphi_\varepsilon, v_\varepsilon, \mu_\varepsilon, \theta_\varepsilon)$ solves (1.2)–(1.7) and converges formally as $\varepsilon \rightarrow 0$ to a limit $(u, \varphi, v, \mu, \theta)$. Furthermore, we suppose that the family of the zero level sets of the functions φ_ε converges as $\varepsilon \rightarrow 0$ to a sharp interface. This interface, at times $t \in [0, T]$ is supposed to be given as a smooth curve $\gamma(t) \subset \Gamma$ which separates the regions $\{\varphi(\cdot, t) = 1\}$ and $\{\varphi(\cdot, t) = -1\}$. By a formal asymptotic analysis, we conclude that the limit functions $(u, \varphi, v, \mu, \theta)$ can be characterized as the solutions of a free boundary problem on the surface Γ , which is again coupled to a diffusion equation in the bulk B . Other examples for this method and more details on formal asymptotic analysis can be found in [2, 4, 9, 19, 21] which is by far not a comprehensive list of references.

The obtained limit problem describes a time-dependent partition of the surface Γ into different phase regions

$$(4.1) \quad \Gamma^+(t) := \{\varphi(\cdot, t) = 1\} \quad \text{and} \quad \Gamma^-(t) := \{\varphi(\cdot, t) = -1\}$$

and the dynamic of the interface $\gamma(t)$ between these two regions. We denote the corresponding separation of the surface-time domain $\Gamma \times (0, T]$ by

$$\mathbf{\Gamma}^\pm := \{(x, t) \in \Gamma \times (0, T] : x \in \Gamma^\pm(t)\}.$$

The limit problem then takes the following form.

Sharp Interface Problem 4.1. The sharp interface model obtained from the formal asymptotic analysis is given by

$$(4.2) \quad \varphi = \pm 1 \quad \text{on } \mathbf{\Gamma}^\pm,$$

$$(4.3) \quad \partial_t u = D\Delta u \quad \text{in } B \times (0, T],$$

$$(4.4) \quad -D\nabla u \cdot \nu = q := c_1 u(1 - v) - c_2 v \quad \text{on } \Gamma \times (0, T],$$

$$(4.5) \quad \Delta_\Gamma \mu = 0 \quad \text{on } \mathbf{\Gamma}^\pm,$$

$$(4.6) \quad \partial_t v = \Delta_\Gamma \theta + q \quad \text{on } \mathbf{\Gamma}^\pm,$$

$$(4.7) \quad \theta = \frac{2}{\delta} (2v - 1 \mp 1) \quad \text{on } \mathbf{\Gamma}^\pm,$$

$$(4.8) \quad 2\mu + \theta = c_0 \kappa_g \quad \text{on } \gamma,$$

$$(4.9) \quad [\mu]_-^+ = 0 \quad \text{on } \gamma,$$

$$(4.10) \quad [\theta]_-^+ = 0 \quad \text{on } \gamma,$$

$$(4.11) \quad -2\mathcal{V} = [\nabla_\Gamma \mu]_-^+ \cdot \nu_\gamma \quad \text{on } \gamma,$$

$$(4.12) \quad -\mathcal{V} = [\nabla_\Gamma \theta]_-^+ \cdot \nu_\gamma \quad \text{on } \gamma,$$

where $[\cdot]^\pm$ is the jump across the interface γ and $\nu_\gamma(x_0, t_0) \in T_{x_0}\Gamma$ denotes the unit normal to $\gamma(t_0)$ in $x_0 \in \gamma(t_0)$, pointing inside $\Gamma^+(t_0)$. The geodesic curvature of $\gamma(t)$ in Γ is denoted by $\kappa_g(\cdot, t)$ and $\mathcal{V}(x_0, t_0)$ denotes the normal velocity of $\gamma(t_0)$ in $x_0 \in \gamma(t_0)$ in direction of $\nu_\gamma(x_0, t_0)$. For its precise definition, let $\gamma_t : U \rightarrow \gamma(t) \subset \Gamma$, $t \in (t_0 - \delta, t_0 + \delta)$ be a smoothly evolving family of local parameterizations of the curves $\gamma(t)$ by arc length over an open interval $U \subset \mathbb{R}$ and let $\gamma_{t_0}(s_0) = x_0$. Then the normal velocity in (x_0, t_0) is given by

$$\mathcal{V}(x_0, t_0) = \left. \frac{d}{dt} \right|_{t_0} \gamma_t(s_0) \cdot \nu_\gamma(x_0, t_0),$$

see also [11].

We first deduce the existence of transition layers between the phase regions. By assuming that the functions $(u_\varepsilon, \varphi_\varepsilon, v_\varepsilon, \mu_\varepsilon, \theta_\varepsilon)$ admit suitable expansions with respect to the parameter ε in the transition layers and in the regions away from the interface respectively, we can then deduce that the limit functions at least formally need to fulfill (4.2)–(4.12).

4.1. Asymptotic analysis: Existence of transition layers and outer expansion. We start our analysis by expanding the solutions to the coupled model in the outer regions, where φ_ε attains values away from zero. We assume that in these regions all functions in (1.2)–(1.7) have expansions of the form

$$f_\varepsilon = \sum_{k=0}^{\infty} \varepsilon^k f_k$$

where $f_\varepsilon = \varphi_\varepsilon, v_\varepsilon, \dots$, etc.

Since we postulated the existence of different phase regions characterized by the values of the limit function φ , we should first address the existence of these phase regions. To this end, we collect all terms of order ε^{-1} in (1.2) and obtain

$$W'(\varphi_0) = 0$$

and as a consequence we obtain $\varphi_0 = \pm 1$ as the only stable solutions. Since φ_0 is the dominant term in the assumed expansion as $\varepsilon \rightarrow 0$, we deduce $\varphi_\varepsilon \rightarrow \pm 1$ as $\varepsilon \rightarrow 0$ and the existence of the claimed transition layers. This justifies (4.1) and (4.2).

The discussion of equations (1.3) and (1.4)–(1.7) is then straightforward. Comparing the terms of order $\mathcal{O}(1)$ in their corresponding equations allows us to deduce (4.3)–(4.7).

Due to the (possibly step) transition between the regions Γ^+ and Γ^- near the interface, the spatial derivatives occurring in the system might contribute terms which are not necessarily of order $\mathcal{O}(1)$ (with respect to ε) in a neighborhood of the interface. This motivates the need for a more detailed analysis of the functions in the neighborhood of the interface which we will address in Section 4.3.

4.2. Coordinates for a neighborhood of the interface. As stated above, we suppose that the zero level sets of φ_ε converge to some (smooth) curve $\gamma(t)$ with inner (wrt. $\Gamma^+(t)$) unit normal field $\nu_\gamma(\cdot, t)$. We then introduce on a small tubular neighborhood N of $\gamma(t)$ a new coordinate system which is more suitable for the analysis in the transition layer. We remark that the construction of these coordinates presented here is more complicated which is due to the fact that N is a neighborhood of $\gamma(t)$ in the manifold Γ . For a similar example, we refer the reader to [17].

As above, let $\gamma_t : U \rightarrow \gamma(t)$ be a local parametrization of the curve $\gamma(t)$ by arc length over an open interval $U \subset \mathbb{R}$. It is then possible to extend γ_t to a local parametrization Ψ_t of N by means of the exponential map from differential geometry.

While details on this map can be found in the literature [12, 13], it is sufficient for our purpose to quickly recall its definition. For a given point $p \in \Gamma$ and a vector $\vec{a} \in T_p\Gamma$, there exists a unique geodesic curve $c_{\vec{a}}$ such that $c_{\vec{a}}(0) = p$ and $c'_{\vec{a}}(0) = \vec{a}$. The exponential map \exp_p in p is then defined for all $\vec{a} \in T_p\Gamma$ for which $c_{\vec{a}}(1)$ exists and is given by $\exp_p(\vec{a}) = c_{\vec{a}}(1)$. Note that for $z \in [0, 1]$ one can easily check $\exp_p(z\vec{a}) = c_{\vec{a}}(z)$.

The distance between a point $x \in \Gamma$ and the interface $\gamma(t)$ is defined as

$$d(x, t) := \inf\{l(c) \mid c : I \rightarrow \Gamma, c \text{ connects } x \text{ and } \gamma(t)\}$$

where $l(c)$ denotes the length of the curve c . Setting

$$\Psi_t(s, r) = \exp_{\gamma_t(s)}(r\nu_\gamma(\gamma_t(s), t)),$$

we obtain that Ψ_t is a parametrization of a neighborhood $N(t)$ of $\gamma(t)$. If we choose $N(t)$ small enough, the properties of the exponential map imply that r is the signed distance between the point $\Psi_t(s, r)$ and $\gamma(t)$, that is for $(x, t) = \Psi_t(s, r) \in N(t)$ we have

$$r = \widehat{d}(x, t) := \begin{cases} d(\Psi_t(s, r), t) & \text{if } r \in \Gamma^+(t) \\ -d(\Psi_t(s, r), t) & \text{if } r \in \Gamma^-(t). \end{cases}$$

For the asymptotic analysis, it is necessary to adapt the parametrization to the length scale of the transition layers. We therefore use the rescaled parametrization

$$(4.13) \quad \Lambda(s, z, t) = \Psi_t(s, \varepsilon z)$$

of $N(t)$, where $z = \frac{r}{\varepsilon}$. In particular, z can be written as a function of x and t .

Let us remark that as $\gamma(t)$ is the zero level set of the signed distance function \widehat{d} , the tangent space of $\gamma(t)$ is the subspace of the tangent space of Γ which is orthogonal to the surface gradient $\nabla_\Gamma \widehat{d}$ and thus the normal vector ν_γ of $\gamma(t)$ is given by $\frac{\nabla_\Gamma \widehat{d}}{\|\nabla_\Gamma \widehat{d}\|_\Gamma}$. Because of

$$0 = \frac{d}{dt} \widehat{d}(\gamma_t(s), t) = \nabla_\Gamma \widehat{d}(\gamma_t(s), t) \cdot \partial_t \gamma_t(s) + \partial_t \widehat{d}(\gamma_t(s), t)$$

we can thus compute

$$\partial_t \gamma_t(s) \cdot \nu = -\frac{\partial_t \widehat{d}(\gamma_t(s), t)}{\|\nabla_\Gamma \widehat{d}(\gamma_t(s), t)\|_\Gamma}$$

and therefore the time derivative $\partial_t z$ on $\gamma(t)$ fulfills

$$\partial_t z = -\varepsilon^{-1} \nu.$$

Remark 4.2 (Gradient, Divergence and Laplace Operator in the new coordinates). From the definition of Λ in (4.13) we see

$$(4.14) \quad \Lambda(s, 0, t) = \gamma_t(s),$$

$$(4.15) \quad \partial_s \Lambda(s, 0, t) = \partial_s \gamma_t(s) = \gamma_t'(s) \text{ and}$$

$$(4.16) \quad \partial_z \Lambda(s, 0, t) = \varepsilon \nu_\gamma(\gamma_t(s)).$$

Furthermore, the curve $r \mapsto \Psi_t(s, r)$ is geodesic by definition and hence we have

$$\mathcal{P} \partial_{zz} \Lambda(s, z, t) = 0$$

where \mathcal{P} is the projection on the tangent space $T_{\Lambda(s, z, t)} \Gamma$ on Γ in $\Lambda(s, z, t)$.

These observations allow us to calculate

$$\begin{aligned} \partial_z (\partial_s \Lambda(s, z, t) \cdot \partial_z \Lambda(s, z, t)) &= \partial_{zs} \Lambda(s, z, t) \cdot \partial_z \Lambda(s, z, t) + \partial_s \Lambda(s, z, t) \cdot \partial_{zz} \Lambda(s, z, t) \\ &= \frac{1}{2} \partial_s |\partial_z \Lambda(s, z, t)|^2 = 0 \end{aligned}$$

since $|\partial_z \Lambda(s, z, t)|^2 = \varepsilon^2$ by definition. The equations (4.15) and (4.16) imply $\partial_s \Lambda(s, 0, t) \cdot \partial_z \Lambda(s, 0, t) = 0$, which yields

$$(4.17) \quad \partial_s \Lambda(s, z, t) \cdot \partial_z \Lambda(s, z, t) = 0.$$

For simplification of the following calculations, we denote the variables s and z by s_1 and s_2 respectively. Given the arguments above, the metric tensor with respect to Λ is given by

$$\begin{aligned} g_{11} &= g_{ss} = \partial_s \Lambda \cdot \partial_s \Lambda, \\ g_{12} &= g_{21} = g_{sz} = g_{zs} = \partial_s \Lambda \cdot \partial_z \Lambda = 0 \text{ and} \\ g_{22} &= g_{zz} = \partial_z \Lambda \cdot \partial_z \Lambda = \varepsilon^2. \end{aligned}$$

The matrix

$$G := \begin{pmatrix} g_{11} & g_{12} \\ g_{21} & g_{22} \end{pmatrix}$$

is thus diagonal and as usual we denote the entries of its inverse G^{-1} by g^{ij} .

For a scalar function $h(x, t) = \widehat{h}(s(t, x), z(t, x), t)$ on N , the surface gradient on $N \subset \Gamma$ is hence expressed by

$$(4.18) \quad \nabla_{\Gamma} h = \sum_{i,j=1}^2 g^{ij} \partial_{s_i} \widehat{h} \partial_{s_j} \Lambda = g^{11} \partial_{s_1} \widehat{h} \partial_{s_1} \Lambda + \frac{1}{\varepsilon^2} \partial_{s_2} \widehat{h} \partial_{s_2} \Lambda = \nabla_{\gamma_{\varepsilon}} \widehat{h} + \frac{1}{\varepsilon} \partial_z \widehat{h} \partial_z \Lambda$$

where $\nabla_{\gamma_{\varepsilon}}$ is the surface gradient on $\gamma_{\varepsilon} = \{\Lambda(s, z, t) | s \in U\}$ for a fixed $z \in [0, 1]$. Similarly,

$$(4.19) \quad \nabla_{\Gamma} \cdot a = \nabla_{\gamma_{\varepsilon}} \cdot \widehat{a} + \frac{1}{\varepsilon} \partial_z \widehat{a} \cdot \partial_z \Lambda$$

for some vector valued function $a(x, t) = \widehat{a}(s(x, t), z(x, t), t)$.

In analogy to the appendix in [2], we calculate the Laplace-Beltrami operator Δ_{Γ} in the new coordinates. Due to the properties of the parametrization $\Lambda(s, z, t)$ which already lead to the diagonal structure of the metric tensor above, we find $\nabla_{\gamma_{\varepsilon}} \widehat{h} \cdot \partial_z \Lambda = 0$ and $\nabla_{\gamma_{\varepsilon}} \widehat{h} \cdot \partial_{zz} \Lambda = 0$. Hence

$$\left(\partial_z \nabla_{\gamma_{\varepsilon}} \widehat{h} \right) \cdot \partial_z \Lambda = \left(\partial_z \nabla_{\gamma_{\varepsilon}} \widehat{h} \right) \cdot \partial_z \Lambda + \nabla_{\gamma_{\varepsilon}} \widehat{h} \cdot \partial_{zz} \Lambda = \partial_z \left(\nabla_{\gamma_{\varepsilon}} \widehat{h} \cdot \partial_z \Lambda \right) = 0$$

and substituting (4.18) in (4.19) we thus compute

$$\begin{aligned} \Delta_{\Gamma} h &= \Delta_{\gamma_{\varepsilon}} \widehat{h} + \frac{1}{\varepsilon} \left(\nabla_{\gamma_{\varepsilon}} \partial_z \widehat{h} \right) \cdot \partial_z \Lambda + \frac{1}{\varepsilon} \partial_z \widehat{h} \nabla_{\gamma_{\varepsilon}} \cdot \partial_z \Lambda \\ &\quad + \frac{1}{\varepsilon} \left(\nabla_{\partial_z \gamma_{\varepsilon}} \widehat{h} \right) \cdot \partial_z \Lambda + \frac{1}{\varepsilon^2} \partial_{zz} \widehat{h} \cdot \partial_z \Lambda + \frac{1}{\varepsilon^2} \partial_z \widehat{h} \partial_{zz} \Lambda \cdot \partial_z \Lambda \\ (4.20) \quad &= \Delta_{\gamma_{\varepsilon}} \widehat{h} + \frac{1}{\varepsilon} \partial_z \widehat{h} \nabla_{\gamma_{\varepsilon}} \cdot \partial_z \Lambda + \frac{1}{\varepsilon^2} \partial_{zz} \widehat{h} \cdot \partial_z \Lambda \end{aligned}$$

where we have used the identities above. Since

$$\partial_{ss} \Lambda \cdot \partial_s \Lambda = \frac{1}{2} \partial_s (\partial_s \Lambda \cdot \partial_s \Lambda) = 0,$$

the curvature vector $\partial_{ss} \Lambda$ of $\gamma(t)$ (seen as a curve in \mathbb{R}^3) is an element in $\text{span}(\partial_z \Lambda, \nu_{\Gamma})$ where ν_{Γ} denotes the direction normal to the surface Γ . The geodesic curvature κ_g of $\gamma(t)$ in Γ is therefore given by

$$\kappa_g = \partial_{ss} \Lambda \cdot \partial_z \Lambda = \partial_s (\partial_s \Lambda \cdot \partial_z \Lambda) - \partial_s \Lambda \cdot \partial_{sz} \Lambda = -\nabla_{\gamma_{\varepsilon}} \cdot \partial_z \Lambda.$$

As in [2], one can derive

$$\begin{aligned} \nabla_{\gamma_{\varepsilon}} \widehat{h} &= \nabla_{\gamma} \widehat{h} + \mathcal{R}_{\varepsilon} \\ \nabla_{\gamma_{\varepsilon}} \cdot \widehat{h} &= \nabla_{\gamma} \cdot \widehat{h} + \mathcal{R}_{\varepsilon} \\ \Delta_{\gamma_{\varepsilon}} \widehat{h} &= \Delta_{\gamma} \widehat{h} + \mathcal{R}_{\varepsilon} \end{aligned}$$

where \mathcal{R}_ε is of higher order in ε . Thus (4.20) reads

$$\begin{aligned} \Delta_\Gamma h &= \Delta_{\gamma_\varepsilon} \widehat{h} - \frac{1}{\varepsilon} \kappa_g \partial_z \widehat{h} + \frac{1}{\varepsilon^2} \partial_{zz} \widehat{h} \cdot \partial_z \Lambda \\ (4.21) \quad &= \Delta_\gamma \widehat{h} - \frac{1}{\varepsilon} \kappa_g \partial_z \widehat{h} + \frac{1}{\varepsilon^2} \partial_{zz} \widehat{h} \cdot \partial_z \Lambda + \mathcal{R}_\varepsilon. \end{aligned}$$

4.3. Asymptotic analysis: Inner expansion. We assume now that the functions in (1.2) - (1.7) have inner expansions on N with respect to the new variables of the form

$$f_\varepsilon(x, t) = F(z, s, t; \varepsilon) = \sum_{k=0}^{\infty} \varepsilon^k F_k(z, s, t)$$

where again $f_\varepsilon = \varphi_\varepsilon, v_\varepsilon, \dots$ etc. Accordingly, the inner expansions for (v, ϕ, μ, θ) will be denoted by (V, Φ, M, Θ) .

In order for the inner and outer expansions to be consistent with each other, we prescribe the following matching conditions as $z \rightarrow \pm\infty$ (again we use F as a placeholder for (V, Φ, M, Θ))

$$(4.22) \quad F_0(t, s, \pm\infty) \sim f_0^\pm(x, t),$$

$$(4.23) \quad \partial_z F_0(t, s, \pm\infty) \sim 0,$$

$$(4.24) \quad \partial_z F_1(t, s, \pm\infty) \sim \nabla_\Gamma f_0^\pm(x, t) \cdot \nu_\gamma$$

where $(x, t) = \Lambda(0, s, t)$ and $f_0^\pm(x, t) = \lim_{\delta \rightarrow 0} f_0(\exp_x(\pm\delta\nu_\gamma), t)$. We refer the reader to [9, 21] and [19] for a derivation of these matching conditions.

We plug these asymptotic expansions in the equations (1.2)-(1.7) and use the results from Remark 4.2 where necessary. Again we collect all terms with the same order in ε . As we assume that the limes $\varepsilon \rightarrow 0$ exists, we require that the terms associated with the leading orders in ε cancel out. The terms of order ε^{-1} in equation (1.2) hence yield the differential equation

$$-\partial_{zz} \Phi_0 + W'(\Phi_0) = 0$$

for Φ_0 . Together with the matching conditions and the condition $\Phi_0(0) = 0$ we deduce

$$(4.25) \quad \Phi_0(z) = \tanh(z) \quad \text{and} \quad \frac{1}{2} |\partial_z \Phi_0|^2(z) = W(\Phi_0)(z).$$

Looking at the conditions imposed by terms of order ε^{-2} , equation (1.6) yields $\partial_{zz} M_0 = 0$ and integrating this equation from $-\infty$ to z implies that M_0 is independent from z if we take the matching condition (4.23) into account. Thus

$$M_0(z = +\infty) = M_0(z = -\infty),$$

which in turn gives (4.9).

In a similar way, we obtain equation (4.10). The terms of order ε^{-2} in (1.7) indeed imply $\partial_{zz} \Theta_0 = 0$ and integrating in z yields

$$(4.26) \quad \partial_z \Theta_0 = 0$$

by the matching conditions. Again we deduce $\Theta_0(z = +\infty) = \Theta_0(z = -\infty)$ and (4.22) yields (4.10).

Let us observe for later use that $[\theta]_-^+ = 0$ directly implies

$$(4.27) \quad [v]_-^+ = 1$$

as we already saw that $[\varphi]_-^+ = 2$.

A second observation is motivated by the study of all terms of order $\mathcal{O}(1)$ in (1.3). We can deduce

$$\Theta_0 = \frac{2}{\delta} (2V_0 - 1 - \Phi_0)$$

and since $\partial_z \Theta_0 = 0$ by (4.26) we therefore obtain

$$(4.28) \quad 2\partial_z V_0(z, s, t) = \partial_z \Phi_0(z).$$

Substituting the inner expansions in (1.6) also yields terms of order ε^{-1} . The resulting equation reads

$$-\mathcal{V}\partial_z \Phi_0 = \partial_{zz} M_1.$$

Equation (4.11) is then obtained from the matching conditions by integrating in z .

Next, we study the terms of order $\mathcal{O}(1)$ in (1.2). Similar to the studies on the related Cahn-Hilliard equation we obtain

$$\begin{aligned} M_0 &= -\partial_{zz} \Phi_1 + \kappa_g \partial_z \Phi_0 + W''(\Phi_0) \Phi_1 - \frac{1}{\delta} (2V_0 - 1 - \Phi_0) \\ &= -\partial_{zz} \Phi_1 + \kappa_g \partial_z \Phi_0 + W''(\Phi_0) \Phi_1 - \frac{1}{2} \Theta_0 \end{aligned}$$

and apply the following solvability condition for Φ_1 derived in [4, Lemma 2.2].

Lemma 4.3 ([4]). *Let $A(z)$ be a bounded function on $-\infty < z < \infty$. Then the problem*

$$\begin{aligned} \partial_{zz} \phi + W''(F_0(z)) \phi &= A(z) & z \in \mathbb{R}, \\ \phi(0) &= 0 & \phi \in L^\infty(\mathbb{R}), \end{aligned}$$

has a solution if and only if

$$\int_{\mathbb{R}} A(z) F_0'(z) dz = 0.$$

It is indeed easy to see that this condition is necessary if one multiplies the equation by F_0' and uses integration by parts. The assertion that the condition is also sufficient can be derived from the method of variation of constants, details are given in [4].

Lemma 4.3 directly yields

$$2M_0 = c_0 \kappa_g - \frac{1}{2} \int_{-\infty}^{\infty} \Theta_0 \partial_z \Phi_0 dz$$

where c_0 is given by

$$c_0 := \int_{-\infty}^{\infty} |\partial_z \Phi_0|^2 dz.$$

Given the fact that Θ_0 is independent of z (see (4.26)) we deduce

$$\int_{-\infty}^{\infty} \Theta_0 \partial_z \Phi_0 dz = \Theta_0 \int_{-\infty}^{\infty} \partial_z \Phi_0 dz = 2\Theta_0.$$

We thus conclude

$$2\mu + \theta = c_0 \kappa_g$$

as we claimed in (4.8).

In order to conclude our analysis, we collect all terms of order ε^{-1} from equation (1.7). We thus have

$$-\mathcal{V}\partial_z V_0 = \partial_{zz} \Theta_1$$

and another integration with respect to z allows us to deduce

$$-\mathcal{V}[v]_-^+ = [\nabla_\Gamma \theta]_-^+ \cdot \nu_\gamma$$

from the matching conditions. Our observation (4.27) on $[v]_-^+$ above hence implies (4.12).

4.4. Free energy inequalities and conservation properties. The discussion of the thermodynamical background in Section 2 can be extended to the sharp interface model (4.2)–(4.12) derived above if one considers the surface free energy

$$(4.29) \quad \begin{aligned} \mathcal{F}(\varphi, v, \gamma) &:= c_0 \int_{\gamma} 1 \, d\mathcal{H}^1 + \frac{1}{2\delta} \int_{\Gamma} (2v - 1 - \varphi)^2 \, d\mathcal{H}^2 \\ &= c_0 \int_{\gamma} 1 \, d\mathcal{H}^1 + \frac{1}{2\delta} \left[\int_{\Gamma^-} (2v)^2 \, d\mathcal{H}^2 + \int_{\Gamma^+} (2v - 2)^2 \, d\mathcal{H}^2 \right] \end{aligned}$$

and the bulk free energy

$$(4.30) \quad \mathcal{F}_b(u) := \frac{1}{2} \int_B u^2 \, dx.$$

In particular, choosing these energies the energy inequality derived in Lemma 2.1 for the diffuse interface model from the second law of thermodynamics has a counterpart in the sharp interface model, i.e.

$$\frac{d}{dt} [\mathcal{F}(\varphi, v, \gamma) + \mathcal{F}_b(u)] \leq \int_{\Gamma} q(\theta - u) \, d\mathcal{H}^2.$$

As the following calculations show, this is mostly due to the relations specified in the equations (4.8)–(4.12) on γ . They come into play since

$$(4.31) \quad \frac{d}{dt} \int_{\gamma} 1 \, d\mathcal{H}^1 = \int_{\gamma} \kappa_g \mathcal{V} \, d\mathcal{H}^1.$$

We refer the reader to Section 5.4 in [12] for a derivation of this identity.

Let us now calculate the time derivative of (4.29) in order to derive the desired energy inequality. Reynolds' transport theorem and (4.31) imply

$$(4.32) \quad \begin{aligned} \frac{d}{dt} \mathcal{F}(\varphi, v, \gamma) &= c_0 \int_{\gamma} \kappa_g \mathcal{V} \, d\mathcal{H}^1 + \frac{1}{2\delta} \frac{d}{dt} \int_{\Gamma} \left(\frac{\delta}{2} \theta \right)^2 \, d\mathcal{H}^2 \\ &= c_0 \int_{\gamma} \kappa_g \mathcal{V} \, d\mathcal{H}^1 + \frac{\delta}{8} \frac{d}{dt} \left(\int_{\Gamma^+} \theta^2 \, d\mathcal{H}^2 + \int_{\Gamma^-} \theta^2 \, d\mathcal{H}^2 \right) \\ &= c_0 \int_{\gamma} \kappa_g \mathcal{V} \, d\mathcal{H}^1 + \frac{\delta}{4} \int_{\Gamma^+} \theta \partial_t \theta \, d\mathcal{H}^2 + \frac{\delta}{4} \int_{\Gamma^-} \theta \partial_t \theta \, d\mathcal{H}^2. \end{aligned}$$

We have used equation (4.10) to derive the last equality. Because of (4.8), the first integral $c_0 \int_{\gamma} \kappa_g \mathcal{V} \, d\mathcal{H}^1$ coincides with $\int_{\gamma} (2\mu + \theta) \mathcal{V} \, d\mathcal{H}^1$. Using (4.11) and (4.12) yields

$$(4.33) \quad \begin{aligned} c_0 \int_{\gamma} \kappa_g \mathcal{V} \, d\mathcal{H}^1 &= - \int_{\gamma} \mu [\nabla_{\Gamma} \mu]_{-}^{+} \cdot \nu_{\gamma} \, d\mathcal{H}^1 - \int_{\gamma} \theta [\nabla_{\Gamma} \theta]_{-}^{+} \cdot \nu_{\gamma} \, d\mathcal{H}^1 \\ &= - \int_{\gamma} \mu \nabla_{\Gamma} \mu^{+} \cdot \nu_{\gamma} \, d\mathcal{H}^1 + \int_{\gamma} \mu \nabla_{\Gamma} \mu^{-} \cdot \nu_{\gamma} \, d\mathcal{H}^1 \\ &\quad - \int_{\gamma} \theta \nabla_{\Gamma} \theta^{+} \cdot \nu_{\gamma} \, d\mathcal{H}^1 + \int_{\gamma} \theta \nabla_{\Gamma} \theta^{-} \cdot \nu_{\gamma} \, d\mathcal{H}^1. \end{aligned}$$

By the divergence theorem for tangential vector fields on manifolds, we see that all integrals equate to integrals over Γ^+ and Γ^- respectively. That is, we find

$$\begin{aligned} - \int_{\gamma} \mu \nabla_{\Gamma} \mu^{+} \cdot \nu_{\gamma} \, d\mathcal{H}^1 &= - \int_{\Gamma^+} \operatorname{div}(\mu \nabla_{\Gamma} \mu) \, d\mathcal{H}^2 \\ &= - \int_{\Gamma^+} |\nabla_{\Gamma} \mu|^2 \, d\mathcal{H}^2 - \int_{\Gamma^+} \mu \Delta_{\Gamma} \mu \, d\mathcal{H}^2 \\ &= - \int_{\Gamma^+} |\nabla_{\Gamma} \mu|^2 \, d\mathcal{H}^2. \end{aligned}$$

The last equation holds because of (4.5). Keeping in mind that the orientation of γ seen as the boundary of Γ^+ differs from the orientation of γ seen as the boundary of Γ^- , similar calculations lead to

$$\int_{\gamma} \mu \nabla_{\Gamma} \mu^{-} \cdot \nu_{\gamma} d\mathcal{H}^1 = - \int_{\Gamma^{-}} |\nabla_{\Gamma} \mu|^2 d\mathcal{H}^2.$$

For the other integrals in (4.33), we use (4.6) and (4.7) to calculate

$$\begin{aligned} - \int_{\gamma} \theta \nabla_{\Gamma} \theta^{+} \cdot \nu_{\gamma} d\mathcal{H}^1 &= - \int_{\Gamma^{+}} |\nabla_{\Gamma} \theta|^2 d\mathcal{H}^2 - \int_{\Gamma^{+}} \theta \Delta_{\Gamma} \theta d\mathcal{H}^2 \\ &= - \int_{\Gamma^{+}} |\nabla_{\Gamma} \theta|^2 d\mathcal{H}^2 - \int_{\Gamma^{+}} \theta (\partial_t v - q) d\mathcal{H}^2 \\ &= - \int_{\Gamma^{+}} |\nabla_{\Gamma} \theta|^2 d\mathcal{H}^2 - \frac{\delta}{4} \int_{\Gamma^{+}} \theta \partial_t \theta d\mathcal{H}^2 + \int_{\Gamma^{+}} \theta q d\mathcal{H}^2 \end{aligned}$$

and the analogue result

$$\int_{\gamma} \theta \nabla_{\Gamma} \theta^{-} \cdot \nu_{\gamma} d\mathcal{H}^1 = - \int_{\Gamma^{-}} |\nabla_{\Gamma} \theta|^2 d\mathcal{H}^2 - \frac{\delta}{4} \int_{\Gamma^{-}} \theta \partial_t \theta d\mathcal{H}^2 + \int_{\Gamma^{-}} \theta q d\mathcal{H}^2.$$

Plugging these findings in (4.33) yields

$$c_0 \int_{\gamma} \kappa_g \mathcal{V} d\mathcal{H}^1 = - \int_{\Gamma} |\nabla_{\Gamma} \mu|^2 d\mathcal{H}^2 - \int_{\Gamma} |\nabla_{\Gamma} \theta|^2 d\mathcal{H}^2 - \frac{\delta}{4} \int_{\Gamma} \theta \partial_t \theta d\mathcal{H}^2 + \int_{\Gamma} \theta q d\mathcal{H}^2$$

and by (4.32) we deduce

$$\begin{aligned} \frac{d}{dt} \mathcal{F}(\varphi, v, \gamma) &= - \int_{\Gamma} |\nabla_{\Gamma} \mu|^2 d\mathcal{H}^2 - \int_{\Gamma} |\nabla_{\Gamma} \theta|^2 d\mathcal{H}^2 + \int_{\Gamma} \theta q d\mathcal{H}^2 \\ &\leq \int_{\Gamma} \theta q d\mathcal{H}^2. \end{aligned}$$

Similarly to the derivation of Lemma 2.1, we also find

$$\frac{d}{dt} \mathcal{F}_b(u) \leq \int_{\Gamma} u q d\mathcal{H}^2.$$

This leads to the free energy inequality for the sharp interface model stated in 4.1,

$$(4.34) \quad \frac{d}{dt} [\mathcal{F}(\varphi, v, \gamma) + \mathcal{F}_b(u)] \leq \int_{\Gamma} q(\theta - u) d\mathcal{H}^2.$$

Furthermore, equation (4.2) and Reynolds' transport theorem allow us to deduce

$$(4.35) \quad \begin{aligned} \frac{d}{dt} \int_{\Gamma} \varphi d\mathcal{H}^2 &= \frac{d}{dt} \int_{\Gamma^{+}(t)} 1 d\mathcal{H}^2 - \frac{d}{dt} \int_{\Gamma^{-}(t)} 1 d\mathcal{H}^2 \\ &= \int_{\gamma(t)} \mathcal{V} \cdot \nu_{\gamma} d\mathcal{H}^2 - \int_{\gamma(t)} \mathcal{V} \cdot \nu_{\gamma} d\mathcal{H}^2 = 0. \end{aligned}$$

We remark that the signs in the above equation depend on the values of φ in $\Gamma^{+}(t)$ and $\Gamma^{-}(t)$ respectively as well as the fact that $\gamma(t)$ is seen as the boundary of $\Gamma^{+}(t)$ for the first integral and as the boundary of $\Gamma^{-}(t)$ for the second integral.

For energy densities chosen according to (4.29) and (4.30), equations (4.3) and (4.4) correspond to the mass balance equation for cytosolic cholesterol (2.11), while the mass balance equation (2.2) for the membrane bound cholesterol corresponds to (4.6). We use these equations to deduce

$$(4.36) \quad \frac{d}{dt} \left[\int_B u dx + \int_{\Gamma} v d\mathcal{H}^2 \right] = 0.$$

Equations (4.35) and (4.36) show that the conservation laws derived in Lemma 2.1 hold for the sharp interface model as well. Equation (4.34) is the analogue to the general energy inequality in

Lemma 2.1 for the sharp interface model, if one chooses the constitutive relations in such a way that the resulting free energy densities lead to (4.29) and (4.30).

5. NUMERICAL SIMULATIONS

In this section we present numerical results for the reduced non-local system (3.8)–(3.11) and for the fully coupled bulk–surface model (1.2)–(1.8). For the first, we propose a discretization which is semi-implicit in time and which is based on surface finite elements in space [14, 15]. The details of the discretization are shown in Section 5.1. We validate the numerical method in Section 5.2 with two benchmark tests and subsequently, in Section 5.3, we present simulation results showing properties of the model. Moreover, in Section 5.4, we present a numerical simulation for a diffuse interface approximation of the fully coupled bulk–surface model (1.2)–(1.8). For a large bulk diffusion coefficient, the results show a good agreement with those obtained for the reduced model in Section 5.3. This further justifies to use numerical simulations for the reduced model in order to study the properties of the original model.

Cahn–Hilliard systems on stationary surfaces have been numerically investigated by parametric finite elements [43], level set techniques [23] and with diffuse interface methods [43] mostly applied for the simulation of spinodal decomposition and coarsening scenarios. For corresponding results on moving surfaces we refer to [16, 36] (sharp interface approach) and [52] (diffuse interface approach), respectively. Recently, a Cahn–Hilliard like system has been numerically studied for the simulation of the influence of membrane proteins on phase separation and coarsening on cell membranes [53].

5.1. Surface FEM Discretization. For the discretization of the reduced system (3.8)–(3.11) with q given by (1.8) we develop a scheme similar to the one in [41], where a related non-local reaction–diffusion system has been numerically treated. To discretize in time, we introduce steps τ_m , $m = 1, \dots, M_T$. Denoting by $\varphi^{(m)}$, $\mu^{(m)}$, $v^{(m)}$, $u^{(m)}$ the time discrete solution at time $t_m = \sum_{l=1}^m \tau_l$, the time discrete weak formulation then reads

$$(5.1) \quad \int_{\Gamma} \frac{\varphi^{(m+1)}}{\tau_{m+1}} \psi + \int_{\Gamma} \nabla_{\Gamma} \mu^{(m+1)} \cdot \nabla_{\Gamma} \psi = \int_{\Gamma} \frac{\varphi^{(m)}}{\tau_{m+1}} \psi,$$

$$(5.2) \quad - \int_{\Gamma} \mu^{(m+1)} \eta + \varepsilon \int_{\Gamma} \nabla_{\Gamma} \varphi^{(m+1)} \cdot \nabla_{\Gamma} \eta + \frac{1}{\varepsilon} \int_{\Gamma} W''(\varphi^{(m)}) \varphi^{(m+1)} \eta - \frac{2}{\delta} \int_{\Gamma} v^{(m+1)} \eta \\ + \frac{1}{\delta} \int_{\Gamma} \varphi^{(m+1)} \eta = \frac{1}{\varepsilon} \int_{\Gamma} (W''(\varphi^{(m)}) \varphi^{(m)} - W'(\varphi^{(m)})) \eta - \frac{1}{\delta} \int_{\Gamma} \eta,$$

$$(5.3) \quad \int_{\Gamma} \frac{v^{(m+1)}}{\tau_{m+1}} \zeta + \frac{4}{\delta} \int_{\Gamma} \nabla_{\Gamma} v^{(m+1)} \cdot \nabla_{\Gamma} \zeta - \frac{2}{\delta} \int_{\Gamma} \nabla_{\Gamma} \varphi^{(m+1)} \cdot \nabla_{\Gamma} \zeta \\ + \int_{\Gamma} (c_1 u^{(m)} + c_2) v^{(m+1)} \zeta = \int_{\Gamma} \frac{v^{(m)}}{\tau_{m+1}} \zeta + \int_{\Gamma} c_1 u^{(m)} \zeta$$

for all $\psi, \eta, \zeta \in H^1(\Gamma)$, where the non-local term

$$(5.4) \quad u^{(m)} = \frac{1}{|B|} \left(M - \int_{\Gamma} v^{(m)} \right)$$

is treated fully explicitly.

For the spatial discretization, we introduce a triangulation Γ_h of the surface Γ , and we use linear surface finite elements to obtain from (5.1)–(5.4) a linear system of equations for the coefficients of the discrete solutions $\mu_h^{(m+1)}$, $\varphi_h^{(m+1)}$, $v_h^{(m+1)}$ with respect to the standard Lagrange basis. The resulting linear system is solved by a direct solver or a stabilized bi-conjugate gradient (BiCGStab) method depending on the number of unknowns. Furthermore, we apply a simple time adaptation

strategy, where time steps τ_{m+1} are chosen (within bounds) inversely proportional to

$$\max_{x \in \Gamma_h} \frac{|\varphi_h^{(m)}(x) - \varphi_h^{(m-1)}(x)|}{\tau_m},$$

see e.g. [43]. The above numerical scheme is implemented in the adaptive FEM toolbox AMDiS [50].

5.2. Benchmark tests. In this section we consider a triangulation $\Gamma_h = S_h^2$ of the unit sphere S^2 , and we use the following set of parameters:

$$(5.5) \quad c_1 = c_2 = 500, \quad \varepsilon = 0.02, \quad M = 5|B| = \frac{20\pi}{3}, \quad \delta = 0.02.$$

5.2.1. Analytic solution for a prescribed right hand side. In order to verify the validity of the above numerical scheme, we define right hand sides for (3.8) and (3.10) such that an analytic solution for the resulting system can be given. To be more precise, we let

$$(5.6) \quad \varphi(x, t) := \tanh\left(\frac{\vartheta(x) + \beta - t}{\sqrt{2}\varepsilon}\right)$$

for $x \in S^2$ and $t \in [0, T]$. Moreover, β is an angle related to the initial value $\varphi(x, 0)$, and by $\vartheta = \vartheta(x)$ we denote the angle given by

$$\vartheta(x) := \arccos(x_3) \in [0, \pi]$$

for $x = (x_1, x_2, x_3) \in S^2$. Furthermore, we let $v(x, t) := \frac{1}{2}(1 + \varphi(x, t))$ such that $\theta = 0$ holds. Then we define $F_1, F_2 : S^2 \times [0, T] \rightarrow \mathbb{R}$ such that

$$(5.7) \quad \partial_t \varphi - \Delta_\Gamma \mu = F_1 \quad \text{on } S^2 \times (0, T],$$

$$(5.8) \quad \mu = -\varepsilon \Delta_\Gamma \varphi + \varepsilon^{-1} W'(\varphi) \quad \text{on } S^2 \times (0, T],$$

$$(5.9) \quad \partial_t v - q(u, v) = F_2 \quad \text{on } S^2 \times (0, T]$$

hold with $u = u(t)$ given by

$$(5.10) \quad u = \frac{3}{4\pi} \left(M - \int_{S^2} v \right).$$

In this way we obtain expressions for F_1 and F_2 , which are incorporated in the numerical scheme described in Section 5.1. Finally, we use the adopted scheme to find approximate numerical solutions φ_h, μ_h, v_h to (5.7)–(5.10) for initial conditions for φ_h, v_h given by corresponding values determined by (5.6) and $v = \frac{1}{2}(1 + \varphi)$. Note that the expression for F_2 involves an integral of φ which is numerically approximated in polar coordinates in every time step.

With the usual Lagrange interpolation operator I_h , we define the relative errors

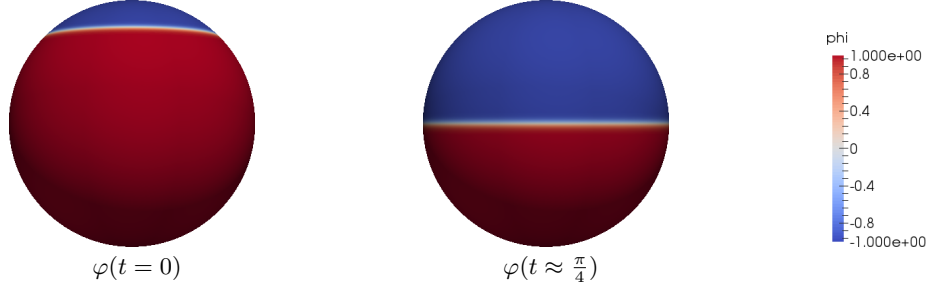
$$e_\infty(t) := \frac{\|I_h \varphi(\cdot, t) - \varphi_h(\cdot, t)\|_{L^\infty(S_h^2)}}{\|\varphi(\cdot, t)\|_{L^\infty(S^2)}},$$

$$e_1(t) := \frac{\|I_h \varphi(\cdot, t) - \varphi_h(\cdot, t)\|_{H^1(S_h^2)}}{\|I_h \varphi(\cdot, t)\|_{H^1(S_h^2)}}$$

of $\varphi_h(\cdot, t)$ in the $L^\infty(S_h^2)$ -, $H^1(S_h^2)$ -norms, respectively, and we consider their values for simulations with $T = \frac{\pi}{4}$, $\beta = -\frac{\pi}{4}$ and different spatial resolutions in Table 1. The results indicate a linear dependence of the $L^\infty(S_h^2)$ - and $H^1(S_h^2)$ -errors, respectively, on the grid-size, as expected for elliptic problems. As a further illustration of this benchmark, in Figure 1, we see contour plots of $\varphi(\cdot, 0)$ and $\varphi(\cdot, T)$, respectively. We remark that in the following we use a grid with 98306 vertices for all simulations with spherical geometry.

number of vertices	6146	24578	98306	393218
$e_\infty(T)$	0.245005	0.0284765	0.0107314	0.00568034
$e_1(T)$	0.2284131488	0.0747088125	0.0407739003	0.0211030453

TABLE 1. Relative errors for simulations of (5.7)–(5.10) with different resolutions.

FIGURE 1. Benchmark simulation with prescribed right hand side in (5.7)–(5.9). Contour plots of initial values of analytic solution (5.6) and of values at time T .

5.2.2. *Validation of $\int v$.* We return to (3.8)–(3.11) and remark that one easily verifies from (3.12) that

$$z := \int_{\Gamma} v$$

fulfills the ODE

$$(5.11) \quad \dot{z} = c_1 \frac{M|\Gamma|}{|B|} - \left(c_1 \frac{|\Gamma|}{|B|} + c_2 + c_1 \frac{M}{|B|} \right) z + \frac{c_1}{|B|} z^2.$$

We compare solutions of the above ODE with

$$\int_{S_h^2} v_h$$

obtained by numerical solution of (5.1)–(5.4), where we have chosen the initial conditions

$$\varphi(\cdot, 0) = -0.25 + \mathcal{R}, \quad v(\cdot, 0) = 0.25.$$

Thereby, $\mathcal{R} : \Gamma_h \rightarrow [-0.001, 0.001]$ provides a perturbation given by an (irregular and nonperiodic) oscillation around zero. In Figure 2, $z_h = \int_{S_h^2} v_h$ obtained by numerical simulation of (5.1)–(5.4) is compared with a numerical solution of the ODE (5.11) with initial condition

$$z(0) = \int_{S^2} v(\cdot, 0)$$

obtained with MapleTM[1]. The excellent agreement further justifies the chosen numerical scheme.

5.3. Simulation results.

5.3.1. *Variation of parameters.* We use the basic set of parameters given in (5.5). Furthermore, we use the initial conditions $\varphi(\cdot, 0) = \hat{\varphi} + \mathcal{R}$, $v(\cdot, 0) = \frac{1}{4}$, where $\hat{\varphi} = -0.5$ and $\mathcal{R} : \Gamma_h \rightarrow [-0.001, 0.001]$ again denotes a perturbation by an (irregular and nonperiodic) oscillation around zero. In Figure 3, we see corresponding results, where contour plots of the discrete solutions $\varphi_h(\cdot, t)$ (first row) and $v_h(\cdot, t)$ (second row) are displayed for various times t . The evolution shows a spinodal decomposition with subsequent interrupted coarsening scenario.

The geometric shape of the particles can drastically change, if one changes the values of $\varphi(\cdot, 0)$. In a second example, we have used $\varphi(\cdot, 0) = 0 + \mathcal{R}$, while all remaining parameters have not been changed. The corresponding numerical results can be seen in Figure 4.

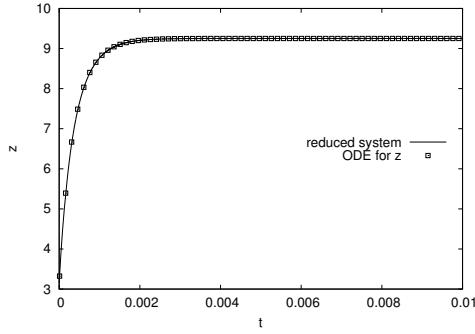


FIGURE 2. Comparison of a numerical solution of the ODE (5.11) with $\int_{S^2} v_h$ obtained by simulation of (3.8)–(3.11).

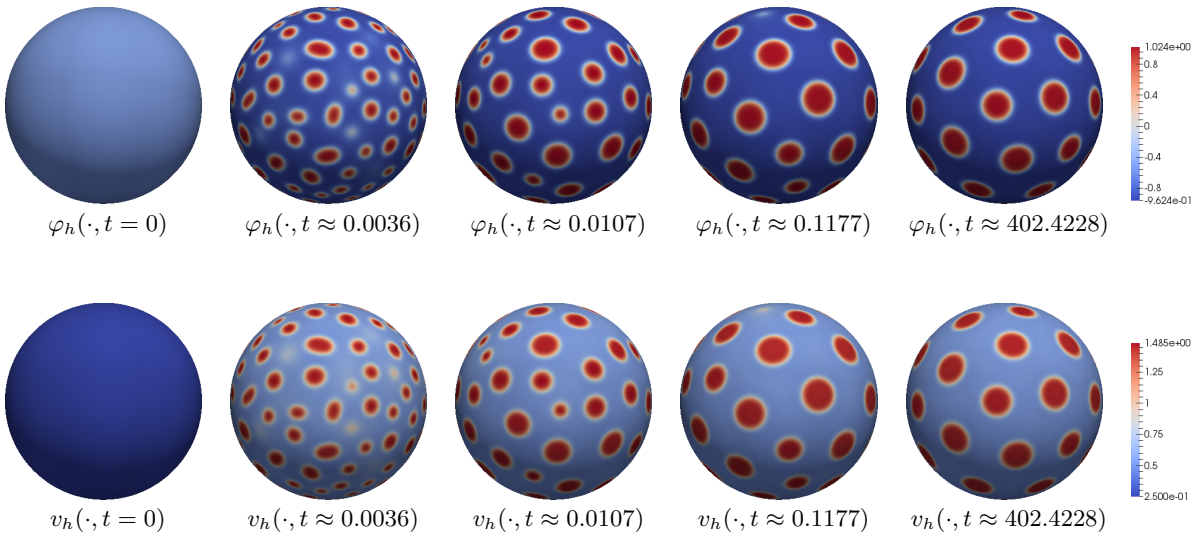


FIGURE 3. Numerical results for $\varphi(\cdot, 0) = -0.5 + \mathcal{R}$. First row: contour plots of $\varphi(\cdot, t)$ for several choices of times t ; second row: corresponding contour plots of $v(\cdot, t)$.

In the following, we compare almost stationary states for simulations with varying parameters, in order to illustrate the properties of the model and its solutions. We use the basic set of parameters for the results shown in Figure 3 and modify one parameter. Let

$$\bar{\varphi} := \int_{\Gamma} \varphi(\cdot, 0) = \int_{\Gamma} \varphi.$$

Varying $\bar{\varphi}$. We change $\bar{\varphi}$ by changing the initial condition for φ , or rather $\hat{\varphi}$. In Figure 5 one observes the almost stationary states from the previous two examples with $\hat{\varphi} = 0$ and $\hat{\varphi} = -0.5$ and examples with intermediate values, where one can see a crossover from circular lipid rafts to stripe like patterns. For $\hat{\varphi} = -0.75$ the system allows for a constant stationary state with order parameter away from the classical phases $\varphi \in \{-1, 1\}$.

Varying δ . For $\hat{\varphi} = -0.5$ we consider almost stationary discrete order parameter φ_h for different values for the parameter δ . In Figure 6, for large δ the almost stationary φ_h has one lipid raft, as one would expect for classical Cahn–Hilliard system on the sphere. For decreasing but still positive values of δ we expect to approach stationary solution of Ohta–Kawasaki based dynamics, as shown in Section 3.4. For a more detailed comparison with almost stationary states of Ohta–Kawasaki based dynamics we refer to the subsequent Section 5.3.2.

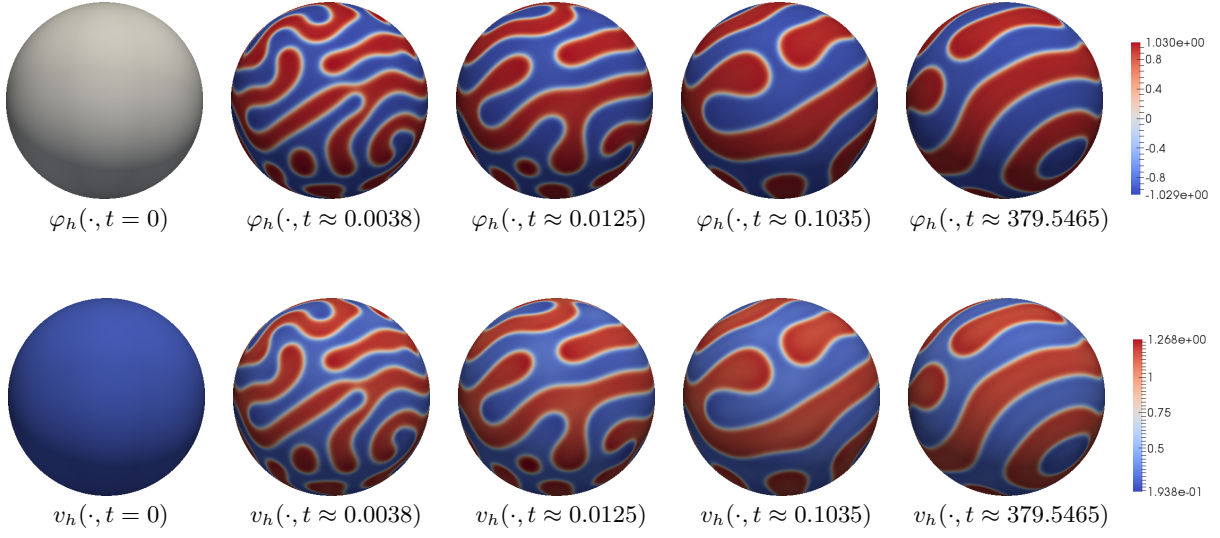


FIGURE 4. Numerical results for $\varphi(\cdot, 0) = 0 + \mathcal{R}$. First row: contour plots of $\varphi(\cdot, t)$ for several choices of times t ; second row: corresponding contour plots of $v(\cdot, t)$.

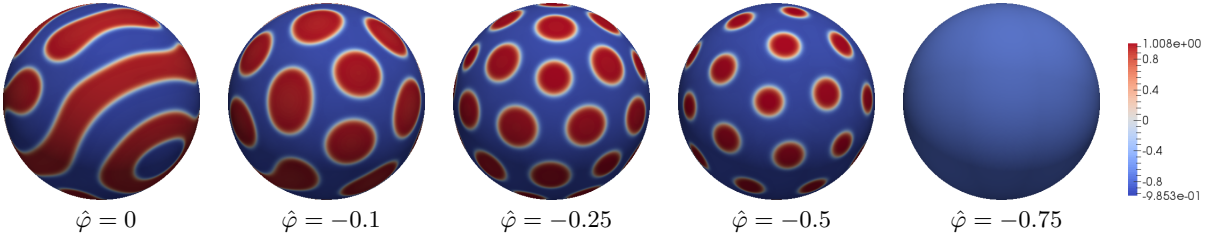


FIGURE 5. Almost stationary discrete solutions φ_h for different values of $\hat{\varphi}$.

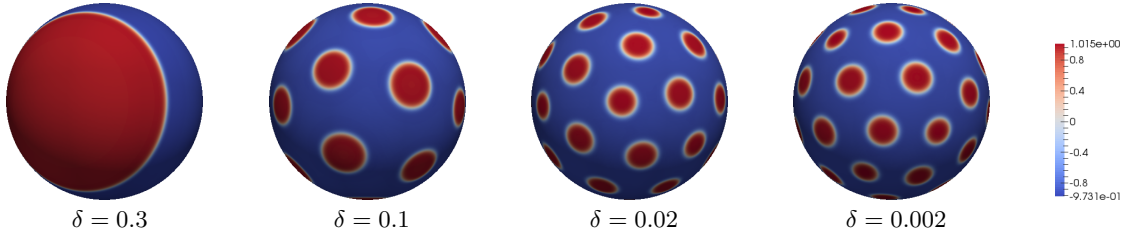
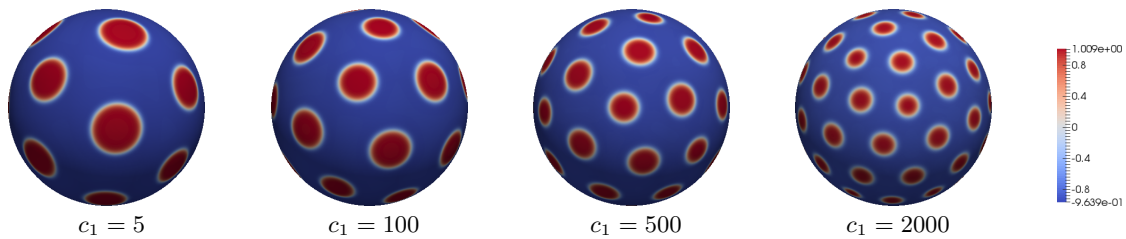
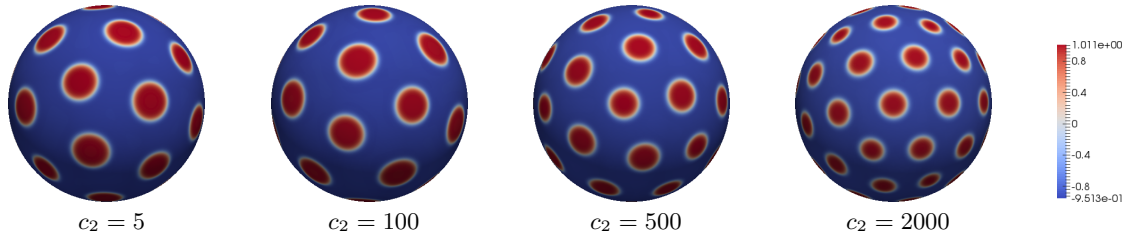


FIGURE 6. Almost stationary discrete solutions φ_h for different values of δ .

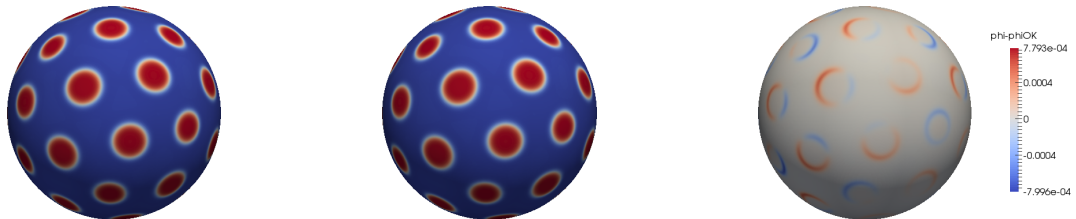
Varying c_1 . Returning to the previous standard parameters $\hat{\varphi} = -0.5$ and $\delta = 0.02$ we investigate the influence of different values of c_1 on the almost stationary discrete states. Increasing c_1 corresponds to increasing the number of lipid rafts as shown in Figure 7.

Varying c_2 . With our standard choice $c_1 = 500$ we obtain for variation of values for c_2 similar results as for the previous examples (varying c_1). In Figure 8, one observes increasing number of rafts of decreasing sizes for increasing c_2 .

From the analysis in Section 3.4 we conclude that increasing c_1 or c_2 corresponds to increasing the non-local energy contribution in the Ohta–Kawasaki functional (3.22), see also (3.23), which is expected to describe the dynamics in the limit $\delta \rightarrow 0$. This fact provides an explanation of the increasing number of particles for increasing c_1, c_2 .

FIGURE 7. Almost stationary discrete solutions φ_h for different values of c_1 .FIGURE 8. Almost stationary discrete solutions φ_h for different values of c_2 .

5.3.2. *Comparison with Ohta–Kawasaki model.* For the result in Figure 9 we have investigated the following scenario. We run a simulation of (3.8)–(3.11) with parameter values as in (5.5) except $\delta = 0.0001$ towards an almost stationary state (see Figure 9, left). With the resulting discrete order parameter φ_h we continue a simulation with Ohta–Kawasaki-based dynamics with parameters according to (3.23) and (3.24) again towards an almost stationary state (see Figure 9, middle). The difference between these two stationary results for φ_h is displayed in Figure 9 (right). These results confirm the analytic results of Section 3.4.

FIGURE 9. Almost stationary φ_h obtained from a simulation of the reduced system (left) and from subsequent Ohta–Kawasaki-based dynamics (middle), difference between the previous numerical solutions (right).

5.3.3. *Non-spherical membrane shape.* In a further example, we show in Figure 10 results with the standard parameter set (5.5) for the case that Γ is not a sphere. One obtains similar patterns as for the sphere. However, this configuration appears to be more stable than the previous spherical ones, where sometimes very slow arrangements could take place. This behavior has not been observed for this geometry. We remark that for this simulation, we have chosen a similar resolution as for the previous examples with spherical geometry.

5.3.4. *Comparison with energy decreasing dynamics.* Here, we study a choice of q leading to an energy decreasing evolution. From the analysis in Section 3.3, we expect that solutions of the system (3.8)–(3.11) generically converge to configurations with one lipid phase concentrated in a single geodesic ball. For this purpose, we choose

$$q = -c(\theta - u)$$

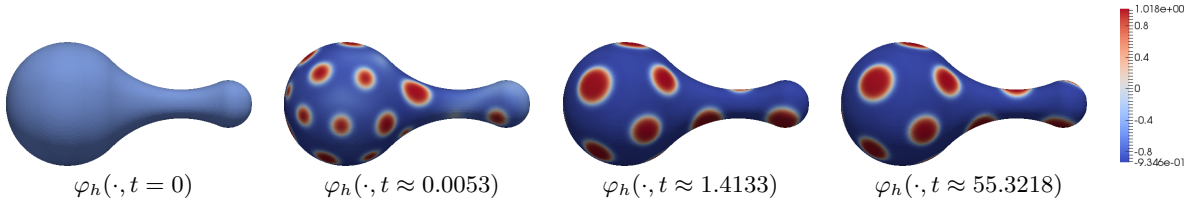


FIGURE 10. Numerical results for a non-spherical surface and $\varphi(\cdot, 0) = -0.5 + \mathcal{R}$. Contour plots of $\varphi(\cdot, t)$ for several choices of times t .

with $c = 500$, corresponding to (2.17) and $f_b(u) = \frac{1}{2}u^2$ in (2.15). The results in this case are displayed in Figure 11 and illustrate the evolution towards an almost stationary state with a single spherical raft particle.

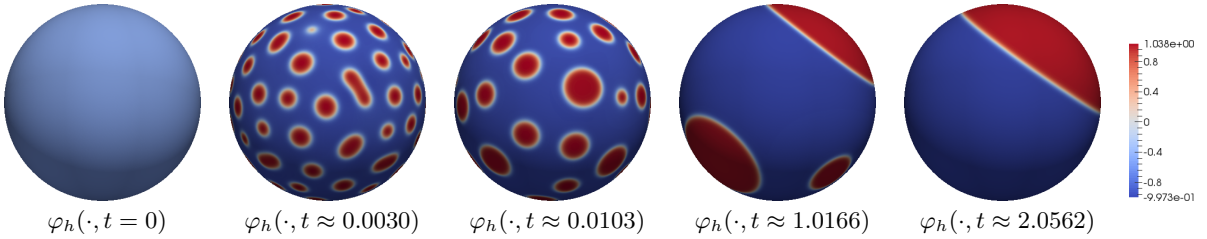


FIGURE 11. Numerical results for a choice of q leading to an energy decreasing evolution and $\varphi(\cdot, 0) = -0.5 + \mathcal{R}$. Contour plots of $\varphi(\cdot, t)$ for several choices of times t .

5.4. Simulation of the full model. For the simulation of the coupled bulk-surface model (1.2)–(1.8), we propose a diffuse interface approximation based on the diffuse approaches for the treatment of PDE's on and inside closed surfaces in [43] and [33], respectively. For a related phase-field description of a coupled bulk-surface reaction-diffusion system, we refer to [42]. Moreover, a further diffuse interface description of a coupled bulk-surface system has been given in [47], and in [3] a diffuse interface approach of a linear coupled elliptic PDE system has been analyzed with respect well-posedness of the diffuse system and convergence towards its sharp interface counterpart.

We choose a domain $\Omega \subset \mathbb{R}^3$ containing \overline{B} and provide a phase-field approximation of (1.2)–(1.7) by

$$(5.12) \quad \psi \partial_t u = D \nabla \cdot (\psi \nabla u) - \varepsilon_g^{-1} b(\psi) q(u, v) \quad \text{in } \Omega \times (0, T],$$

$$(5.13) \quad b(\psi) \partial_t \varphi = \nabla \cdot (b(\psi) \nabla \mu) \quad \text{in } \Omega \times (0, T],$$

$$(5.14) \quad b(\psi) \mu = -\varepsilon \nabla \cdot (b(\psi) \nabla \varphi) + \varepsilon^{-1} b(\psi) W'(\varphi) - \delta^{-1} b(\psi) (2v - 1 - \varphi) \quad \text{in } \Omega \times (0, T],$$

$$(5.15) \quad b(\psi) \partial_t v = \frac{4}{\delta} \nabla \cdot (b(\psi) \nabla v) - \frac{2}{\delta} \nabla \cdot (b(\psi) \nabla \varphi) + b(\psi) q(u, v) \quad \text{in } \Omega \times (0, T],$$

where the phase-field function $\psi : \Omega \rightarrow \mathbb{R}$ describing the geometry, that is B and Γ , is given by

$$(5.16) \quad \psi(x) := \frac{1}{2} \left(1 - \tanh \left(\frac{3r(x)}{\varepsilon_g} \right) \right)$$

for a (small) real number $\varepsilon_g > 0$ and a signed distance r to Γ being negative in B . Note that ψ is obtained by smearing out the characteristic function χ_B of B on a length proportional to ε_g . Moreover, $b = b(\psi) := 36\psi^2(1-\psi)^2$ is small outside the diffuse interface region.

We use a semi-implicit adaptive FEM discretization (see [42]) and choose $\Omega = (-2, 2)^3$ with all solutions assumed Ω -periodic, $\varepsilon_g = \frac{1}{8}$, $D = 100$. All otherwise degenerate mobility functions appearing in second order terms in (5.12)–(5.15) are regularized by addition of a parameter

$\delta_r = 10^{-5}$. The resulting linear system is solved by a stabilized bi-conjugate gradient (BiCGStab) solver. The numerical scheme is implemented in AMDiS [50]. Moreover, we apply the parameters in (5.5) and initial conditions as in Section 5.3 and additionally $u(\cdot, 0) = 4.25$ corresponding to $M = \frac{20\pi}{3}$ in (5.5). In Figure 12 we see plots of $\varphi_h(\cdot, t)|_{\{\psi_h = \frac{1}{2}\}}$ for various times t , where ψ_h is obtained by replacing r by a discrete signed distance r_h in (5.16). The results are in good qualitative agreement with the results in Section 5.3 (see Figure 3) and hence further justify the reduced model formally obtained in the limit $D \rightarrow \infty$.

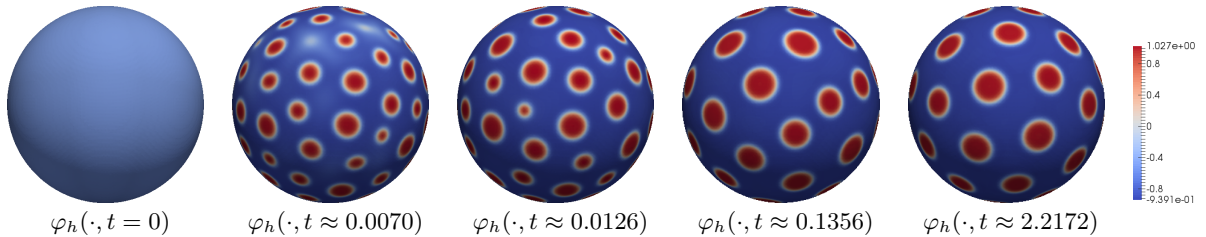


FIGURE 12. Numerical results for diffuse interface approximation of the full model (1.2)–(1.8). Contour plots of $\varphi(\cdot, t)|_{\{\psi_h = \frac{1}{2}\}}$ for several choices of times t .

6. CONCLUSIONS

We have presented a model for lipid raft formation that extends in particular the model by Gómez, Sagués and Reigada [22]. The key new aspect in our work is an explicit account for the cholesterol dynamics in the cytosol, which leads to a complex system of partial differential equations both in the bulk and on the cell membrane. These are coupled by an outflow condition for the cytosolic cholesterol and a source term in the surface membrane equation, determined by a constitutive relation. These considerations lead to an interesting and complex mathematical model. The surface equations combine a Cahn–Hilliard type evolution equation for an order parameter and an equation for the surface cholesterol. The latter is a diffusion equation including a cross-diffusion term and an additional (nonlocal) term. In the bulk we have a diffusion equation with a Robin-type boundary condition that couples both systems.

We have shown that our model can be derived from thermodynamical conservation laws and free energy inequalities for bulk and surface processes. Depending on the specific choice of the exchange term we obtain a total free energy decrease or not, which can be seen as a distinction between equilibrium (closed system) and non-equilibrium (open system) type models. The analysis of both classes reveals striking differences in the behavior: whereas equilibrium-type models only support the formation of macrodomains and connected phases, a prototypical choice of a non-equilibrium model leads to the formation of raft-like structures.

These findings are the result of both a (formal) qualitative mathematical analysis and careful numerical simulations. More precisely, in a certain parameter regime (large interaction strength between lipid and cholesterol) we have demonstrated that stationary states of the prototypical non-equilibrium model are close to stationary states of the Ohta–Kawasaki model, whereas in the case of equilibrium models stationary states coincide with stationary states for a surface Cahn–Hilliard equation.

For a better understanding of the (complex) model asymptotic reductions are instrumental. We in particular justify the sharp interface limit of the model, that is the reduction when the parameter ε (related to the width of transition layers between the distinct lipid phases) tends to zero. Moreover, we have derived a simplified model by taking the cytosolic diffusion (typically much larger than the lateral membrane diffusion) to infinity. This reduction leads to a non-local model that only includes variables on the surface membrane.

Numerical simulation show that, depending on the parameter choices, uniformly distributed circular microdomains or stripe pattern that stretch out over the membrane emerge. A justification of the numerical scheme and implementation is presented and the dependence on the various parameters is analyzed. Further evidence for the connection with the Ohta–Kawasaki dynamics (with specific parameters that are in functional relation to the parameters of our model) is given.

Our results support the belief that non-equilibrium processes are indeed essential for microdomain formation. On the other hand, emerging structures are—in the long-time behavior—very regular and uniform, in contrast to the picture of a persisting redistribution of location and sizes of rafts observed in experiments. Thermal fluctuations and/or the interaction with proteins on the membrane have to be taken into account to obtain this more complex behavior. Our contribution presents a solid basis for such extensions.

REFERENCES

- [1] Maple™16, maple is a trademark of waterloo maple inc.
- [2] H. Abels, H. Garcke, and G. Grün. Thermodynamically consistent, frame indifferent diffuse interface models for incompressible two-phase flows with different densities. *Math. Models Methods Appl. Sci.*, 22(3):1150013, 40, 2012.
- [3] H. Abels, K. F. Lam, and B. Stinner. Analysis of the diffuse domain approach for a bulk-surface coupled PDE system. 2015. arXiv:1502.04902.
- [4] M. Alfaro, D. Hilhorst, and H. Matano. The singular limit of the Allen-Cahn equation and the Fritz-Nagumo system. *Journal of Differential Equations*, 245:505 – 565, 2008.
- [5] H. W. Alt and I. Pawlow. Thermodynamical models of phase transitions with multicomponent order parameter. In *Trends in applications of mathematics to mechanics (Lisbon, 1994)*, volume 77 of *Pitman Monogr. Surveys Pure Appl. Math.*, pages 87–98. Longman, Harlow, 1995.
- [6] M. Bahiana and Y. Oono. Cell dynamical system approach to block copolymers. *Phys. Rev. A (3)*, 41:6763–6771, 1990.
- [7] F. S. Bates and G. H. Fredrickson. Block copolymers - designer soft materials. *Physics today*, 52(2):32–38, 1999.
- [8] D. Brown and E. London. Functions of lipid rafts in biological membranes. *Annual review of cell and developmental biology*, 14(1):111–136, 1998.
- [9] G. Caginalp and P. C. Fife. Dynamics of layered interfaces arising from phase boundaries. *SIAM J. Appl. Math.*, 48(3):506–518, 1988.
- [10] T. L. Chantawansri, A. W. Bosse, A. Hexemer, H. D. Ceniceros, C. J. García-Cervera, E. J. Kramer, and G. H. Fredrickson. Self-consistent field theory simulations of block copolymer assembly on a sphere. *Physical Review E*, 75(3):031802, 2007.
- [11] K. Deckelnick, G. Dziuk, and C. M. Elliott. Computation of geometric partial differential equations and mean curvature flow. *Acta Numer.*, 14:139–232, 2005.
- [12] M. P. do Carmo. *Differential geometry of curves and surfaces*. Prentice-Hall, Inc., Englewood Cliffs, N.J., 1976. Translated from the Portuguese.
- [13] M. P. do Carmo. *Riemannian geometry*. Mathematics: Theory & Applications. Birkhäuser Boston, Inc., Boston, MA, 1992. Translated from the second Portuguese edition by Francis Flaherty.
- [14] G. Dziuk and C. M. Elliott. Surface Finite Elements for Parabolic Equations. *J. Comput. Math.*, 25(4):385–407, 2007.
- [15] G. Dziuk and C. M. Elliott. Finite element methods for surface PDEs. *Acta Numer.*, 22:289–396, 2013.
- [16] C. M. Elliott and B. Stinner. Modeling and computation of two phase geometric biomembranes using surface finite elements. *J. Comput. Phys.*, 229(18):6585–6612, 2010.
- [17] C. M. Elliott and B. Stinner. A surface phase field model for two-phase biological membranes. *SIAM J. Appl. Math.*, 70(8):2904–2928, 2010.
- [18] J. Fan, M. Sammalkorpi, and M. Haataja. Formation and regulation of lipid microdomains in cell membranes: Theory, modeling, and speculation. *FEBS Letters*, 584(9):1678–1684, 2010.
- [19] P. C. Fife. *Dynamics of internal layers and diffusive interfaces*, volume 53 of *CBMS-NSF Regional Conference Series in Applied Mathematics*. Society for Industrial and Applied Mathematics (SIAM), Philadelphia, PA, 1988.
- [20] L. Foret. A simple mechanism of raft formation in two-component fluid membranes. *Europhysics Letters*, 71(3):508–514, 2005.
- [21] H. Garcke and B. Stinner. Second order phase field asymptotics for multi-component systems. *Interfaces Free Bound.*, 8(2):131–157, 2006.

- [22] J. Gómez, F. Sagués, and R. Reigada. Actively maintained lipid nanodomains in biomembranes. *Phys Rev E Stat Nonlin Soft Matter Phys*, 77(2 Pt 1):021907, Feb 2008.
- [23] J. Greer, A. Bertozzi, and G. Sapiro. Fourth order partial differential equations on general geometries. *J. Comput. Phys.*, 216(1):216–246, 2006.
- [24] M. E. Gurtin. On a nonequilibrium thermodynamics of capillarity and phase. *Quart. Appl. Math.*, 47(1):129–145, 1989.
- [25] M. E. Gurtin. Generalized Ginzburg-Landau and Cahn-Hilliard equations based on a microforce balance. *Phys. D*, 92(3-4):178–192, 1996.
- [26] M. E. Gurtin, E. Fried, and L. Anand. *The mechanics and thermodynamics of continua*. Cambridge University Press, Cambridge, 2010.
- [27] J. P. Keener. Activators and inhibitors in pattern formation. *Stud. Appl. Math.*, 59(1):1–23, 1978.
- [28] O. A. Ladyzhenskaya and N. N. Ural'tseva. *Linear and quasilinear elliptic equations*. Translated from the Russian by Scripta Technica, Inc. Translation editor: Leon Ehrenpreis. Academic Press, New York-London, 1968.
- [29] L. Leibler. Theory of microphase separation in block copolymers. *Macromolecules*, 13(6):1602–1617, 1980.
- [30] P.-F. Lenne and A. Nicolas. Physics puzzles on membrane domains posed by cell biology. *Soft Matter*, 5(15):2841–2848, 2009.
- [31] J. Li, J. Fan, H. Zhang, F. Qiu, P. Tang, and Y. Yang. Self-assembled pattern formation of block copolymers on the surface of the sphere using self-consistent field theory. *The European Physical Journal E: Soft Matter and Biological Physics*, 20(4):449–457, 2006.
- [32] J. Li, H. Zhang, and F. Qiu. Self-consistent field theory of block copolymers on a general curved surface. *The European Physical Journal E*, 37(3):1–11, 2014.
- [33] X. Li, J. Lowengrub, A. Rätz, and A. Voigt. Solving PDEs in complex geometries: a diffuse domain approach. *Commun. Math. Sci.*, 7(1):81–107, 2009.
- [34] I.-S. Liu. *Continuum mechanics*. Advanced Texts in Physics. Springer-Verlag, Berlin, 2002.
- [35] M. W. Matsen and M. Schick. Stable and unstable phases of a diblock copolymer melt. *Physical Review Letters*, 72(16):2660, 1994.
- [36] M. Mercker, A. Marciniak-Czochra, T. Richter, and D. Hartmann. Modeling and computing of deformation dynamics of inhomogeneous biological surfaces. *SIAM J. Appl. Math.*, 73(5):1768–1792, 2013.
- [37] W.-M. Ni. *The mathematics of diffusion*, volume 82 of *CBMS-NSF Regional Conference Series in Applied Mathematics*. Society for Industrial and Applied Mathematics (SIAM), Philadelphia, PA, 2011.
- [38] Y. Nishiura and I. Ohnishi. Some mathematical aspects of the micro-phase separation in diblock copolymers. *Phys. D*, 84(1-2):31–39, 1995.
- [39] T. Ohta and K. Kawasaki. Equilibrium morphology of block polymer melts. *Macromolecules*, 19:2621–2632, 1986.
- [40] P. Podio-Guidugli. Models of phase segregation and diffusion of atomic species on a lattice. *Ric. Mat.*, 55(1):105–118, 2006.
- [41] A. Rätz and M. Röger. Turing instabilities in a mathematical model for signaling networks. *J. Math. Biol.*, 65(6-7):1215–1244, 2012.
- [42] A. Rätz and M. Röger. Symmetry breaking in a bulk-surface reaction-diffusion model for signaling networks. *Nonlinearity*, 27:1805–1827, 2014.
- [43] A. Rätz and A. Voigt. PDE's on surfaces — a diffuse interface approach. *Comm. Math. Sci.*, 4(3):575–590, 2006.
- [44] K. Simons and E. Ikonen. Functional rafts in cell membranes. *Nature*, 387(6633):569–572, Jun 1997.
- [45] P. Sternberg and K. Zumbrun. Connectivity of phase boundaries in strictly convex domains. *Arch. Rational Mech. Anal.*, 141(4):375–400, 1998.
- [46] M. J. Swamy, L. Ciani, M. Ge, A. K. Smith, D. Holowka, B. Baird, and J. H. Freed. Coexisting domains in the plasma membranes of live cells characterized by spin-label esr spectroscopy. *Biophysical journal*, 90(12):4452–4465, 2006.
- [47] K. Teigen, X. Li, J. Lowengrub, F. Wang, and A. Voigt. A diffuse-interface approach for modeling transport, diffusion and adsorption/desorption of material quantities on a deformable interface. *Commun. Math. Sci.*, 7(4):1009–1037, 2009.
- [48] S. L. Veatch and S. L. Keller. Separation of Liquid Phases in Giant Vesicles of Ternary Mixtures of Phospholipids and Cholesterol. *Biophys. J.*, 85:3074–3083, 2003.
- [49] S. L. Veatch and S. L. Keller. Seeing spots: complex phase behavior in simple membranes. *Biochim Biophys Acta*, 1746(3):172–185, Dec 2005.
- [50] S. Vey and A. Voigt. AMDiS — Adaptive multidimensional simulations. *Comput. Visual. Sci.*, 10:57–67, 2007.
- [51] B. Vorselaars, J. U. Kim, T. L. Chantawansri, G. H. Fredrickson, and M. W. Matsen. Self-consistent field theory for diblock copolymers grafted to a sphere. *Soft Matter*, 7(11):5128–5137, 2011.

- [52] X. Wang and Q. Du. Modelling and simulations of multi-component lipid membranes and open membranes via diffuse interface approaches. *J. Math. Biol.*, 56(3):347–371, 2008.
- [53] T. Witkowski, R. Backofen, and A. Voigt. The influence of membrane bound proteins on phase separation and coarsening in cell membranes. *Phys. Chem. Chem. Phys.*, 14:14509–14515, 2012.
- [54] A. Yethiraj and J. C. Weisshaar. Why are lipid rafts not observed in vivo? *Biophysical journal*, 93(9):3113–3119, 2007.